

**NATIONAL ADVISORY COMMITTEE
FOR AERONAUTICS**

REPORT 1333

**ATTENUATION IN A SHOCK TUBE DUE TO
UNSTEADY-BOUNDARY-LAYER ACTION**

By **HAROLD MIRELS**



1957

REPORT 1333

**ATTENUATION IN A SHOCK TUBE DUE TO
UNSTEADY-BOUNDARY-LAYER ACTION**

By HAROLD MIRELS

**Lewis Flight Propulsion Laboratory
Cleveland, Ohio**

National Advisory Committee for Aeronautics

Headquarters, 1512 H Street NW., Washington 25, D. C.

Created by Act of Congress approved March 3, 1915, for the supervision and direction of the scientific study of the problems of flight (U. S. Code, title 50, sec. 151). Its membership was increased from 12 to 15 by act approved March 2, 1929, and to 17 by act approved May 25, 1948. The members are appointed by the President and serve as such without compensation.

JAMES H. DOOLITTLE, Sc. D., Vice President, Shell Oil Company, *Chairman*

LEONARD CARMICHAEL, Ph. D., Secretary, Smithsonian Institution, *Vice Chairman*

ALLEN V. ASTIN, Ph. D., Director, National Bureau of Standards.
PRESTON R. BASSETT, D. Sc.

DETLEV W. BRONK, Ph. D., President, Rockefeller Institute for
Medical Research.

FREDERICK C. CRAWFORD, Sc. D., Chairman of the Board,
Thompson Products, Inc.

WILLIAM V. DAVIS, JR., Vice Admiral, United States Navy,
Deputy Chief of Naval Operations (Air).

PAUL D. FOOTE, Ph. D., Assistant Secretary of Defense, Re-
search and Engineering. (Appointed member of Committee
Oct. 22, 1957.)

WELLINGTON T. HINES, Rear Admiral, United States Navy,
Assistant Chief for Procurement, Bureau of Aeronautics.

JEROME C. HUNSAKER, Sc. D., Massachusetts Institute of
Technology.

CHARLES J. MCCARTHY, S. B., Chairman of the Board, Chance
Vought Aircraft, Inc.

DONALD L. PUTT, Lieutenant General, United States Air Force,
Deputy Chief of Staff, Development.

JAMES T. PYLE, A. B., Administrator of Civil Aeronautics.

FRANCIS W. REICHELDERFER, Sc. D., Chief, United States
Weather Bureau.

EDWARD V. RICKENBACKER, Sc. D., Chairman of the Board,
Eastern Air Lines, Inc.

LOUIS S. ROTHSCHILD, Ph. B., Under Secretary of Commerce for
Transportation.

THOMAS D. WHITE, General, United States Air Force, Chief of
Staff.

HUGH L. DRYDEN, Ph. D., *Director*

JOHN F. VICTORY, LL. D., *Executive Secretary*

JOHN W. CROWLEY, JR., B. S., *Associate Director for Research*

EDWARD H. CHAMBERLIN, *Executive Officer*

HENRY J. E. REID, D. Eng., Director, Langley Aeronautical Laboratory, Langley Field, Va.

SMITH J. DEFRANCE, D. Eng., Director, Ames Aeronautical Laboratory, Moffett Field, Calif

EDWARD R. SHARP, Sc. D., Director, Lewis Flight Propulsion Laboratory, Cleveland, Ohio

WALTER C. WILLIAMS, B. S., Chief, High-Speed Flight Station, Edwards, Calif.

CONTENTS

	Page
SUMMARY.....	1
INTRODUCTION.....	1
ANALYSIS.....	2
Generation of Waves by Mass Sources.....	2
Generation of Waves by Unsteady-Boundary-Layer Action.....	3
ATTENUATION IN A SHOCK TUBE.....	3
Shock Attenuation Formulas.....	3
Limiting Solution for Weak Shocks.....	5
Air-Air Shock Tube with $T_4 = T_1 = 520^\circ \text{ R.}$	5
RESULTS AND DISCUSSION.....	7
Comparison with Experiments of Reference 6.....	7
Comparison with Theory of Reference 6.....	8
CONCLUDING REMARKS.....	9
APPENDIXES	
A—SYMBOLS.....	10
B—CHARACTERISTIC-LINE GEOMETRY AND SOME INTEGRALS.....	10
C—INTERACTION OF PRESSURE WAVES WITH INTERFACES.....	11
D—LAMINAR BOUNDARY LAYER BEHIND WAVE.....	12
E—TURBULENT BOUNDARY LAYER BEHIND WAVE.....	13
F—DEVELOPMENT OF ATTENUATION FORMULAS.....	14
G—IDEAL SHOCK-TUBE RELATIONS.....	15
H—REYNOLDS NUMBERS AND TRANSITION.....	16
I—GENERATION OF PRESSURE WAVES BY WALL SHEAR AND HEAT ADDITION.....	17
REFERENCES.....	18
TABLE I.—EVALUATION OF $I_N = \int_0^1 \frac{z^N dz}{1+bz-cz^2}$	18

REPORT 1333

ATTENUATION IN A SHOCK TUBE DUE TO UNSTEADY-BOUNDARY-LAYER ACTION¹

By HAROLD MIRELS

SUMMARY

A method is presented for obtaining the attenuation of a shock wave in a shock tube due to the unsteady boundary layer along the shock-tube walls. It is assumed that the boundary layer is thin relative to the tube diameter and induces one-dimensional longitudinal pressure waves whose strength is proportional to the vertical velocity at the edge of the boundary layer. The contributions of the various regions in a shock tube to shock attenuation are indicated.

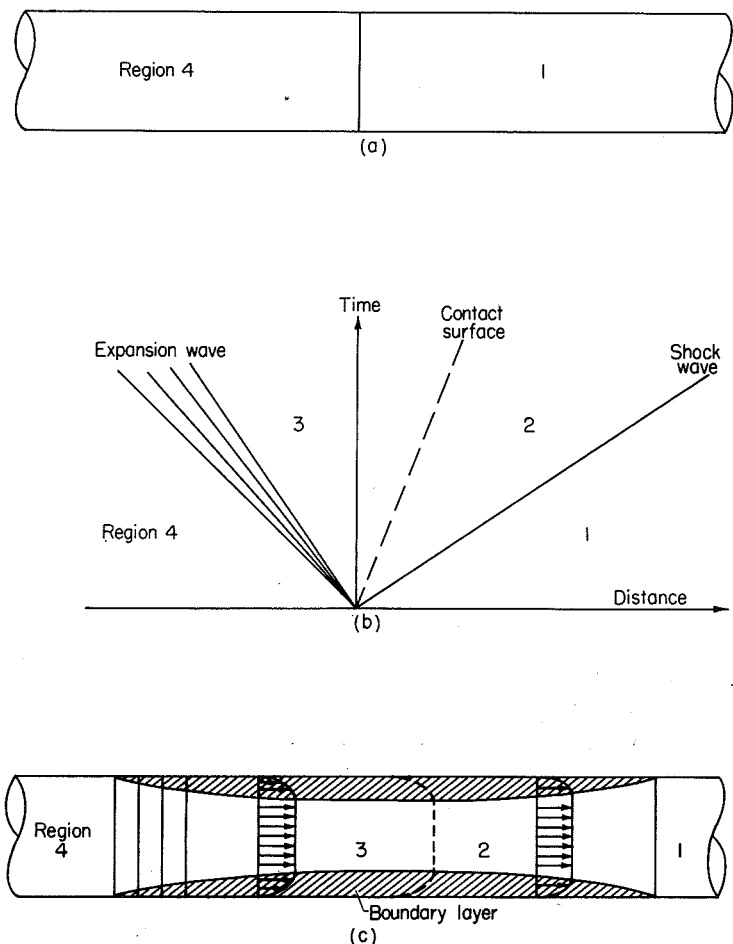
The method is shown to be in reasonably good agreement with existing experimental data.

INTRODUCTION

A shock tube consists of a fluid at high pressure (region 4 of fig. 1 (a)) separated by a diaphragm from a fluid at low pressure (region 1). When the diaphragm bursts, a shock wave propagates into region 1 while an expansion wave propagates into region 4. A time-distance plot of these waves under ideal conditions is indicated in figure 1 (b). Regions 2 and 3 have the same velocity and pressure but have different temperatures. The interface between regions 2 and 3 is referred to as a contact surface. The analysis of the flow for perfect fluids is straight-forward (see, for example, ref. 1). In an actual shock tube, however, viscosity and heat conduction cannot be ignored. These lead to a boundary layer along the walls of the shock tube, as indicated in figure 1 (c). The boundary layer introduces non-uniformities into the shock tube. Analytical studies of this boundary layer are presented in references 2 to 6. One of the important consequences of the wall boundary layer is that it generates weak pressure waves which catch up with and attenuate the shock wave propagating into region 1. This attenuation has been studied experimentally and analytically in the work of references 1, 4, 5, and 6, and is the subject of the present report. It is assumed that the boundary layer is thin relative to the shock-tube diameter. This is a practical restriction, since most shock tubes are designed so that the core of potential flow is relatively uniform in order to permit aerodynamic tests.

A few remarks concerning previous shock-wave-attenuation analyses are appropriate. In reference 4, the coordinate system is defined so that the shock wave is stationary. The flow between the shock wave and the contact surface is considered as a one-dimensional steady flow so that at each

instant the mass flow through the shock wave equals the mass flow at the contact surface. If the mass flow at the contact surface is known at each instant, the corresponding shock strength can be found. The mass flow at the contact surface is determined from the local boundary-layer displacement thickness and free-stream conditions corresponding to an unattenuated shock. However, it can be shown that free-stream conditions do not remain constant at the contact surface (because of perturbations induced by the boundary layer). Moreover, the method of reference 4



(a) Shock tube before diaphragm burst.
(b) Wave diagram for perfect fluid.
(c) Flow in shock tube with real fluid.

FIGURE 1.—Shock-tube phenomena.

¹ Supersedes NACA TN 3278, "Attenuation in a Shock Tube Due to Unsteady-Boundary-Layer Action," by Harold Mirels, 1956.

does not take into account the existence of weak pressure waves between the contact surface and the shock wave. Since it is precisely these pressure waves which are responsible for shock attenuation, the method of reference 4 cannot be expected to give accurate quantitative results. It does, however, indicate some of the important parameters involved. Reference 1 uses the method of reference 4 in its studies of shock attenuation. At best, qualitative agreement with experiment is indicated.

In reference 6, the flow perturbations due to the boundary layer are considered in detail. At each section of the shock tube, the velocity and temperature variations associated with the boundary layer are averaged across the tube to provide an equivalent one-dimensional flow. The wall shear and heat addition due to dissipation and heat transfer at the walls (all found from boundary-layer theory) are assumed to act on this equivalent one-dimensional flow, their action resulting in the generation of one-dimensional pressure waves propagating in both the upstream and downstream directions. By integrating along characteristic lines, the attenuation of the shock propagating into region 1 is then found. The theoretical trends appeared to be in good agreement with the particular experimental results reported therein.

Reference 5 considers the flow in a coordinate system which is stationary with respect to the shock. The unsteady nature of the flow between the shock wave and the contact discontinuity is associated with the receding of the contact surface with respect to the shock wave. Weak pressure waves are assumed to be generated just in front of the receding contact surface. The magnitude of these waves is obtained by a one-dimensional averaging procedure similar to that of reference 6. These waves overtake the shock and result in attenuation. The method of reference 5 ignores the contribution of region 3 and cannot be expected to yield good quantitative agreement with experiment.

Of the previous reports on shock attenuation, reference 6 appears to give the best agreement with experiment. However, it can be shown that the method of reference 6 does not give a completely valid representation of the wave phenomena induced by the boundary layer along the shock-tube wall. The deficiency of reference 6 is mainly associated with its use of wall shear in the determination of the perturbation pressure waves generated by the wall boundary layer. It is well recognized that the effect of a boundary layer on its external flow is directly related to the vertical velocity at the edge of the boundary layer. For example, reference 7, which is concerned with the Rayleigh (impulsive-plate) problem for a compressible fluid, shows that the boundary layer generates pressure waves in the external flow which are equivalent to those which are produced if the wall moves normal to itself with a velocity equal to the vertical velocity at the edge of the boundary layer. The nonzero pressure gradient over a flat plate moving at high speeds (because of the finite displacement thickness of the boundary layer) is an equivalent steady-flow phenomenon (e. g., ref. 8). Thus, a proper way

to find the waves generated by the unsteady wall boundary layer in a shock tube is to base the calculation on the vertical velocity at the edge of the boundary layer. Such an analysis is presented herein. The quantitative results for shock attenuation thus obtained would be expected to differ from those of reference 6. The comparison between the method of reference 6 and that of the present report is discussed more fully in the main body of the report and in the appendix titled GENERATION OF PRESSURE WAVES BY WALL SHEAR AND HEAT ADDITION.

ANALYSIS

One-dimensional flow with mass sources is treated, and the waves generated by these sources are derived. The waves generated by unsteady-boundary-layer action in a tube are found, assuming that the process can be considered as a one-dimensional unsteady flow. The application to the shock-tube problem is then indicated.

GENERATION OF WAVES BY MASS SOURCES

Consider one-dimensional uniform flow in a tube of constant cross-sectional area. Assume that weak mass sources, uniformly distributed across each cross section, are present and perturb the flow. Denote the net perturbation of a quantity (from the uniform-flow conditions) by Δ . (See appendix A for definition of symbols.) The equations of motion are

$$\left. \begin{aligned} \rho \left(\frac{\partial \Delta u}{\partial t} + u \frac{\partial \Delta u}{\partial x} \right) &= - \frac{\partial \Delta p}{\partial x} \quad (\text{Momentum}) \\ \frac{\partial \Delta \rho}{\partial t} + \rho \frac{\partial \Delta u}{\partial x} + u \frac{\partial \Delta \rho}{\partial x} &= m \quad (\text{Continuity}) \\ \Delta p &= a^2 \Delta \rho \quad (\text{Isentropy}) \end{aligned} \right\} \quad (1)$$

where $m = m(x, t)$ is the rate of mass addition per unit cross-sectional area per unit x . The presence of the sources generates waves. Let the superscripts + and - indicate perturbations associated with waves moving in the + x - and - x -directions, respectively. If ξ, τ designates integration variables for x, t , the solution for the net perturbation at any point x, t may be expressed as

$$\Delta p \equiv \Delta p^+ + \Delta p^- \quad (2a)$$

$$\begin{aligned} \Delta u &\equiv \Delta u^+ + \Delta u^- \\ &= \frac{1}{\rho a} (\Delta p^+ - \Delta p^-) \end{aligned} \quad (2b)$$

$$\Delta \rho = \frac{1}{a^2} \Delta p \quad (2c)$$

where

$$\begin{aligned} \Delta p^+ &= \frac{a}{2(1+M)} \int_{-\infty}^x m \left(\xi, t - \frac{x-\xi}{a+u} \right) d\xi \\ \Delta p^- &= \frac{a}{2(1-M)} \int_x^{\pm\infty} m \left(\xi, t - \frac{\xi-x}{a-u} \right) d\xi \end{aligned}$$

The integrations are conducted along the characteristic lines $\tau = t - (x - \xi)/(a + u)$ and $\tau = t - (\xi - x)/(a - u)$ in the ξ, τ plane. The upper limit on the integral for Δp^- is $+\infty$ or $-\infty$ depending on whether $M < 1$ or $M > 1$, respectively. Equation (2b) incorporates the acoustic relations $\Delta p^+ = \rho a \Delta u^+$ and $\Delta p^- = -\rho a \Delta u^-$.

GENERATION OF WAVES BY UNSTEADY-BOUNDARY-LAYER ACTION

Consider a tube of uniform cross section to have flexible walls such that a small normal velocity v can be generated at the walls. This is equivalent to mass entering the tube at the rate $\oint \rho v dl$, per unit x , where the integral is taken around the perimeter of the tube cross-sectional area. If the flow in the tube is considered as one-dimensional,² the equivalent source strength is

$$m = \left. \begin{aligned} & \frac{\rho v l}{A} \\ & = \frac{4 \rho v}{d} \end{aligned} \right\} \quad (3)$$

where $d \equiv 4A/l$ is the hydraulic diameter, and $v = v(x, t)$. The expression for Δp can then be written as

$$\frac{\Delta p}{p} = \frac{2\gamma}{ad} \left[\frac{1}{1+M} \int_{-\infty}^x v \left(\xi, t - \frac{x-\xi}{a+u} \right) d\xi + \frac{1}{1-M} \int_x^{\pm\infty} v \left(\xi, t - \frac{\xi-x}{a-u} \right) d\xi \right] \quad (4)$$

Similar expressions can be written for Δu and $\Delta \rho$. In the case of waves induced by boundary-layer action, the v in equation (4) refers to the normal velocity at the edge of the boundary layer. Note that a positive v results in compression waves, while a negative v results in expansion waves.

ATTENUATION IN A SHOCK TUBE

Equation (4) can be applied to find the attenuation in a shock tube. The details of the analysis are described in appendixes B to F. The resulting formulas for shock attenuation are presented in the following section. The limiting solution for weak shocks and a numerical solution for an air-air shock tube are also indicated.

SHOCK ATTENUATION FORMULAS

The flow in a shock tube is assumed to consist of the ideal basic flow plus small perturbations due to the boundary layer. Ideal shock-tube flow relations are summarized in appendix G. The expansion wave of the ideal flow is assumed to have negligible thickness and to propagate into

² If the flow through the tube cannot be considered as one-dimensional, it is necessary to consider each element of tube surface as an elemental wave source of strength proportional to the local value of v . The net wave strength at any point in the tube is found from an integration over the entire tube surface.

In the problem of attenuation in a shock tube, the shock wave is considered to be uniform, laterally, at each value of x , but to decrease in strength with increases in x . Hence, a one-dimensional analysis is permissible. Actually, small lateral variations of shock strength exist, particularly near the walls, since the boundary layer immediately behind the shock exerts a three-dimensional effect on shock strength. These lateral variations are ignored herein.

The shape of the shock wave was previously studied (ref. 9). It was assumed that region 2 was infinite in extent (i. e., region 3 was neglected), and the problem was considered as a steady-flow problem in a coordinate system moving with the speed of the undisturbed shock. It was found that the shock wave assumes a parabolic shape, but that appreciable shock curvature is restricted to a region near the wall less than a boundary-layer thickness in extent.

region 4 with velocity $u = -a_4$, as indicated in figure 2. Let point d of figure 2 represent an arbitrary point on the shock-wave characteristic. The problem is to find the net pressure perturbation behind the shock (i. e., $\Delta p_{2,d}$). This requires an integration of equation (4) along all the characteristic lines which contribute to $\Delta p_{2,d}$. The major contribution to $\Delta p_{2,d}$ comes from characteristic lines bd , bc , and ab . Hence, these are the characteristic lines considered in the present analysis (as is indicated in appendix B). Integrating along these characteristic lines permits $\Delta p_{2,d}$ to be expressed as

$$\frac{1}{F} \frac{a_2 d}{2\gamma_2} \frac{\Delta p_{2,d}}{p_2} = \left[\frac{1}{1+M_2} \int_{\xi_b}^x v_2 d\xi + \frac{C}{1-M_2} \int_{\xi_b}^{\xi_c} v_2 d\xi + \frac{\gamma_{32} D}{a_{32}(1+M_3)} \int_{\xi_a}^{\xi_b} v_3 d\xi \right] \left(1 - CE \frac{\Delta p_{2,c}}{\Delta p_{2,d}} \right)^{-1} \quad (5)$$

Equation (5) is derived in appendix F. The notation is defined in appendixes A and F. The term $CE \Delta p_{2,c}/\Delta p_{2,d}$ represents the contribution to $\Delta p_{2,d}$ of all the characteristic lines other than bd , bc , and ab (appendix F).

If the boundary layer in region 2 is wholly laminar or wholly turbulent, the boundary-layer solution for v_2 is known (appendixes D and E). Similarly, if the boundary layer in region 3 is wholly laminar or wholly turbulent, the solution for v_3 is known (appendixes D and E). For these special cases, the integrals of equation (5) can be readily evaluated. Thus, if the boundary layers in regions 2 and 3 are both laminar, equation (5) becomes (from eqs. (F6) and (F7) with $n_2 = n_3 = 1/2$)

$$\sqrt{\frac{u_s}{u_2}} \sqrt{\frac{d}{x}} \sqrt{\frac{a_2 d}{v_2}} \frac{\Delta p_{2,d}}{p_2} = \frac{-4\gamma_2 L_2 F}{\left[1 + \frac{1 - (u_s/a_2)}{M_2} \right]^{1/2}} \left\{ 1 + C \frac{\xi_c}{x} - \frac{D\gamma_{32} M_2}{a_{32}} \left[\frac{1 + \frac{1 - (u_s/a_2)}{M_2}}{1 + M_3 + a_{43}} \right] (v_{32})^{1/2} L_{32} \right\} \left[1 - CE \left(\frac{\xi_c}{x} \right)^{1/2} \right]^{-1} \quad (6)$$

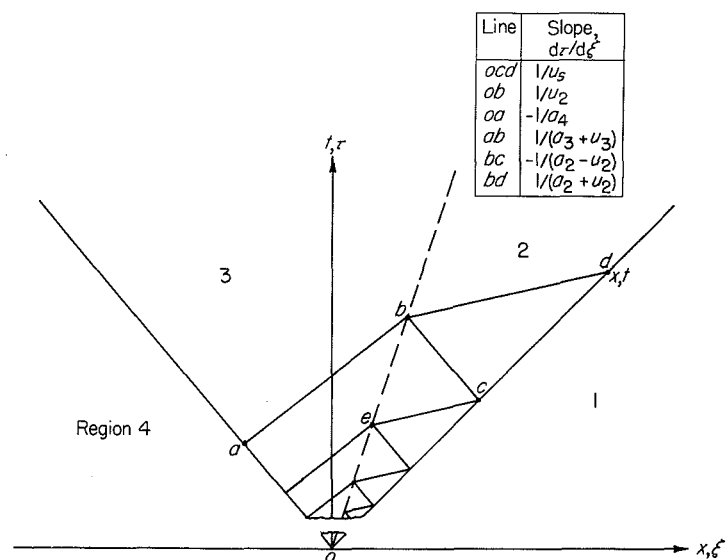


FIGURE 2.—Characteristic lines appropriate for study of attenuation in shock tube.

where L_2 and L_3 are found from appendix D. If the boundary layers in regions 2 and 3 are both turbulent, equation (5) becomes (from eqs. (F6) and (F7) with $n_2=n_3=1/5$)

$$\left(\frac{u_s}{u_2}\right)^{7/5} \left(\frac{d}{x}\right)^{4/5} \left(\frac{a_2 d}{v_2}\right)^{1/5} \frac{\Delta p_{2,d}}{p_2} = \frac{-2.50\gamma_2 L_2 F\left(\frac{u_s}{a_2}\right)^{3/5}}{\left[1 + \frac{1 - (u_s/a_2)}{M_2}\right]^{1/5}} \left\{ 1 + C \frac{\xi_c}{x} - \frac{D\gamma_{32} M_2 \left[1 + \frac{1 - (u_s/a_2)}{M_2}\right]}{a_{32} (1 + M_3 + a_{43})} \right\} \left\{ \left[1 - CE \left(\frac{\xi_c}{x}\right)^{4/5}\right]^{-1} \right\} \quad (7)$$

where L_2 and L_3 are found from appendix E. The other perturbation quantities directly behind the shock can be found from $\Delta p_{2,d}/p_2$ and normal shock relations. For example, utilizing equations (C4) and (C5) gives

$$\begin{aligned} \frac{\Delta u_{2,d}}{u_2} &= \frac{2\gamma_1 M_s^2 - (\gamma_1 - 1)}{4\gamma_1 M_s^2} \frac{M_s^2 + 1}{M_s^2 - 1} \frac{\Delta p_{2,d}}{p_2} \\ \frac{\Delta \rho_{2,d}}{\rho_2} &= \frac{2\gamma_1 M_s^2 - (\gamma_1 - 1)}{\gamma_1 M_s^2 [(\gamma_1 - 1)M_s^2 + 2]} \frac{\Delta p_{2,d}}{p_2} \\ \frac{\Delta T_{2,d}}{T_2} &= \frac{\Delta p_{2,d}}{p_2} \frac{\Delta \rho_{2,d}}{\rho_2} \quad (\text{Eq. of state}) \end{aligned}$$

Note that the perturbations directly behind the shock are *not* isentropically related except for the limit as M_s approaches 1. This is due to the fact that a perturbation of shock strength creates an entropy perturbation. (The particles between the shock wave and the contact surface have entropy perturbations whose magnitude depends on the strength of the shock at the instant each particle passed through it. To the order of the present analysis, these entropy perturbations do not interact with the longitudinal wave system induced by the wall boundary layer.)

Expressions similar to equations (6) and (7) can be found for the mixed cases $n_2=1/2$, $n_3=1/5$ and $n_2=1/5$, $n_3=1/2$. For other boundary-layer characteristics (such as transition from laminar to turbulent flow in the middle of regions 2 or 3), it is necessary to integrate equation (5) with the corresponding v distribution. Reliable criteria for determining the transition points in shock-tube boundary layers have not yet been established. A crude tentative method for estimating the transition points in regions 2 and 3 is presented in appendix H. It is pointed out therein that the Reynolds numbers at point b , computed separately for regions 2 and 3, can be used as an index to determine whether the boundary layers in regions 2 and 3 are primarily laminar or turbulent, respectively. The values of $Re_{2,b}$ and $Re_{3,b}$, as defined in appendix H, can be obtained from figure 3 for the case where the gas in region 1 is air at 520° R.

The present theory requires that the boundary layer be thin relative to the shock-tube diameter. The boundary-layer thickness in region 2 is defined by equations (D5) and (E3) for laminar and turbulent boundary layers, respectively. The laminar-boundary-layer thickness δ_2 is taken to correspond to $u/u_2=0.99$, while the turbulent-boundary-layer

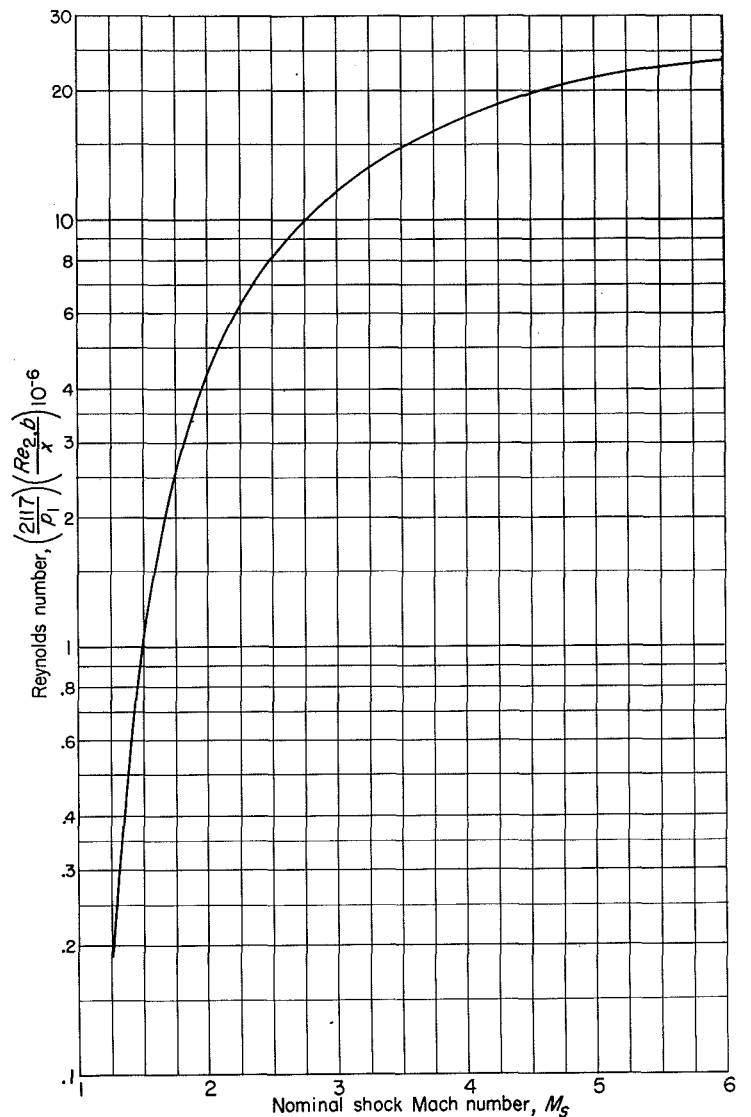
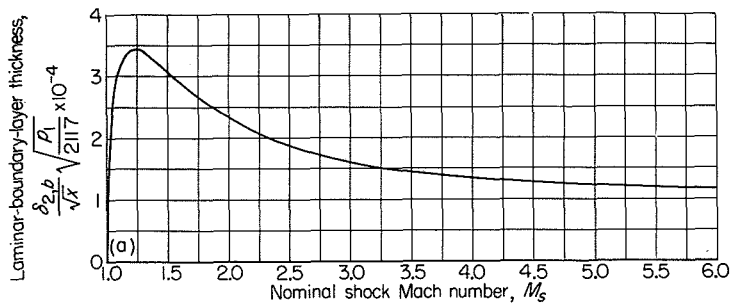


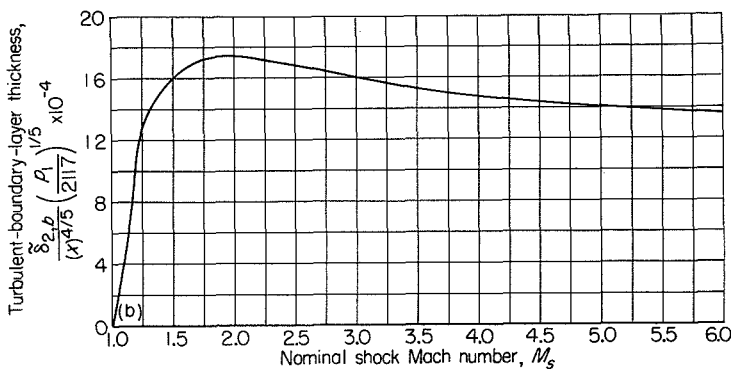
FIGURE 3.—Reynolds number at point b for air in region 1 at 520° R. $Re_{3,b} = v_{23} Re_{2,b}$ (appendix H).

thickness δ_2 is taken to be the value obtained from a Kármán-Pohlhausen-type integral solution. Considering conditions along characteristic lines, the maximum boundary-layer thickness occurs at point b of region 2. Values of $\delta_{2,b}$ and $\delta_{3,b}$ are plotted as a function of M_s in figure 4 for the case where the gas in region 1 is air at 520° R.

It is previously noted, in connection with equation (4), that a positive v results in the generation of compression waves, while a negative v results in the generation of expansion waves. From the boundary-layer theory of appendices D and E it can be seen that, apart from dissipation and heat-transfer effects, v_2 is negative and v_3 is positive. Thus, the boundary layer in region 2 induces expansion waves (which attenuate the shock), while the boundary layer in region 3 induces compression waves (which accelerate the shock). Dissipation and heat transfer modify these results. Dissipation tends to increase v in both regions 2 and 3. Heat transfer from the wall to the boundary layer increases v . Heat transfer from the boundary layer to the wall decreases v . In region 2 the heat transfer is from the boundary layer to



(a) Laminar case (eq. (D5)).



(b) Turbulent case (eq. (E3)).

FIGURE 4.—Boundary-layer thickness at point *b* in region 2. Gas in region 1 is air at 520° R; wall is assumed a perfect conductor ($T_{2,w}=T_1$).

the wall (ref. 2) and leads to larger negative values of v_2 and therefore more shock attenuation. In region 3 the heat transfer is from the wall to the fluid for a weak expansion wave and from the fluid to the wall for a strong expansion wave (ref. 2). Thus, for a weak expansion wave, heat transfer in region 3 tends to generate compression waves (thus accelerating the shock). For a strong expansion wave, the heat transfer in region 3 tends to induce expansion waves (which attenuate the shock). The net effect of all these factors is to attenuate the shock wave. The relative magnitudes of the various terms in equations (6) and (7) are noted later in a numerical example.

LIMITING SOLUTION FOR WEAK SHOCKS

For M_s approaching 1, equations (6) and (7) take on the following forms:

Laminar case:

$$\left(\frac{u_s}{u_2} \frac{d}{x} \frac{a_2 d}{v_2}\right)^{1/2} \frac{\Delta p_{2,d}}{p_2} = \frac{-8\gamma_1}{\sqrt{\pi(\gamma_1+1)}} \left(1 + \frac{\gamma_1-1}{\sqrt{\sigma_1}}\right) \quad (\text{for } T_{2,w}=T_1) \quad (8a)$$

$$= \frac{-8\gamma_1}{\sqrt{\pi(\gamma_1+1)}} \quad (\text{for } T_{2,w}=T_{2,r}) \quad (8b)$$

Turbulent case:

$$\left(\frac{u_s}{u_2}\right)^{3/5} \left(\frac{d}{x}\right)^{3/5} \left(\frac{a_2 d}{v_2}\right)^{3/5} \frac{\Delta p_{2,d}}{p_2} = \frac{-0.115\gamma_1^2}{[2(\gamma_1+1)]^{3/5}} \quad (\text{for } T_{2,w}=T_1) \quad (9a)$$

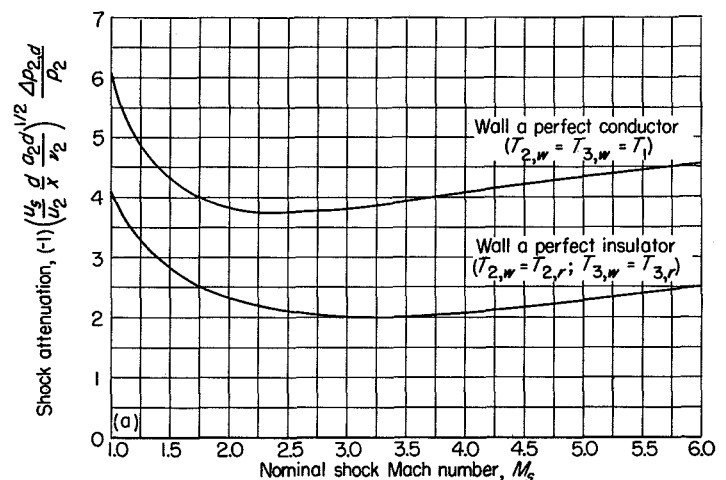
$$= \frac{-0.115\gamma_1}{[2(\gamma_1+1)]^{3/5}} \quad (\text{for } T_{2,w}=T_{2,r}) \quad (9b)$$

The condition $T_{2,w}=T_1$ (eqs. (8a) and (9a)) corresponds to the case where the shock-tube wall is a perfect conductor

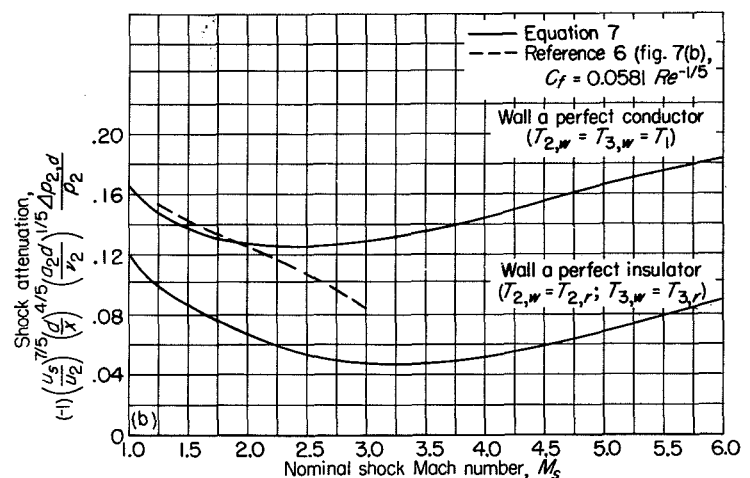
(assuming that the fluid in region 1 is in thermal equilibrium with the wall). Note that taking $T_{2,w}$ equal to T_1 means that the wall remains at its original temperature and that heat is transferred from the fluid (of region 2) to the wall. The condition $T_{2,w}=T_{2,r}$ (eqs. (8b) and (9b)) corresponds to the case wherein the wall is a perfect insulator or has a very low heat capacity. When the shock-tube wall is a metal, the assumption $T_{2,w}=T_1$ should give very accurate results, as discussed in reference 2 (particularly since weak shocks are now being considered). Results for both $T_{2,w}=T_1$ and $T_{2,w}=T_{2,r}$ are given so as to define the upper and lower bounds of the heat-transfer effect on shock attenuation. The attenuation is greater, by a factor of approximately γ_1 , when there is heat transfer as compared with the insulated-wall case. (The factor is exactly γ_1 for the turbulent case and approximately γ_1 for the laminar case, the latter depending on the value of σ_1).

AIR-AIR SHOCK TUBE WITH $T_1=T_2=520^\circ \text{ R}$

Equations (6) and (7) were evaluated numerically for an air-air shock tube with $T_2=T_1=520^\circ \text{ R}$. It was assumed that $\sigma=0.70$ and $\gamma=1.4$. The results for the laminar and turbulent cases are summarized in figure 5. Both the



(a) Laminar case (eq. (6)).



(b) Turbulent case (eq. (7)).

FIGURE 5.—Attenuation in air-air shock tube. $T_1=T_2=520^\circ \text{ R}$; Prandtl number σ , 0.70; ratio of specific heats γ , 1.4.

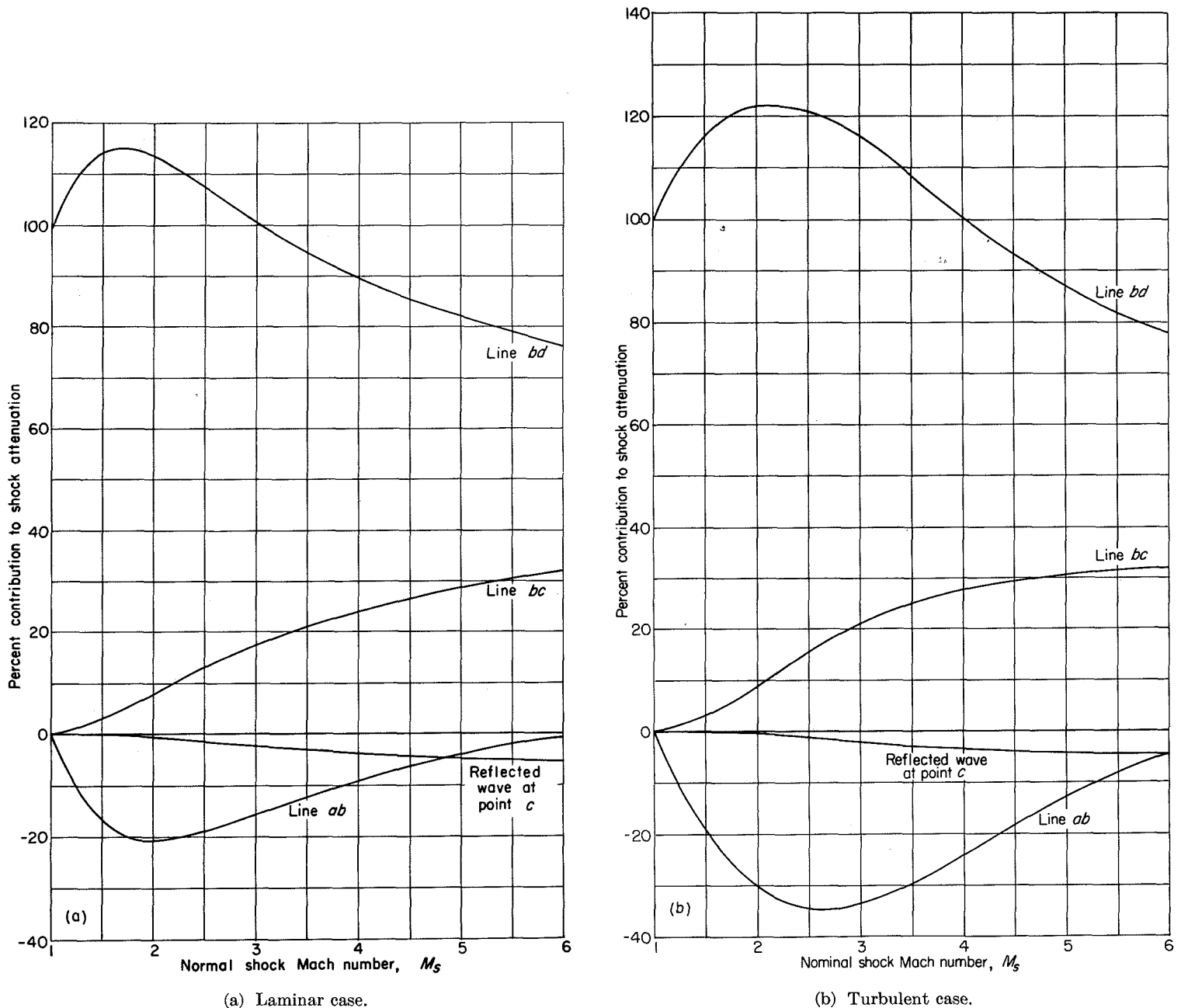


FIGURE 6.—Percent contribution to shock attenuation of characteristic lines of figure 2. Air-air shock tube; $T_1 = T_4 = T_{2,w} = T_{3,w} = 520^\circ \text{ R}$; Prandtl number σ , 0.70; ratio of specific heats γ , 1.4.

insulated-wall case ($T_{2,w} = T_{2,r}$; $T_{3,w} = T_{3,r}$) and the case where the wall is a perfect conductor ($T_{2,w} = T_{3,w} = T_1 = T_4$) are noted therein. When the shock-tube wall is a metal, the assumption that the wall is a perfect conductor should give accurate results except possibly for very strong waves (e. g., ref. 2).

The relative contribution to the net attenuation of the various terms in equations (6) and (7) is indicated in figure 6 for the $T_{2,w} = T_{3,w} = T_1 = T_4$ case. In particular, the percent contribution of the integrations along the characteristic lines bd , ab , and bc and of the reflected wave at point c are indicated therein. (The reflected wave at point c represents the contribution of all the characteristic lines in figure 2 other than lines bd , ab , and bc , as is mentioned in appendix F.) For weak shocks, the major contribution to shock attenua-

tion comes from the integration along line bd . With increasing M_s , the contribution of the characteristic line bc increases gradually to a value of about 30 percent at $M_s = 6.0$. The integration along line ab leads to compression waves (which tend to accelerate the shock) and therefore is negative in figure 6. Its value decreases to about -20 percent at $M_s \approx 2.0$ for the laminar case and to about -35 percent at $M_s \approx 2.75$ for the turbulent case, and then increases with increases in M_s . (The influence of characteristic line ab may be somewhat overestimated in the present analysis because of the assumption of an expansion wave of zero thickness.) The contribution of the reflected wave at point c varies from a value of zero at $M_s = 1$ to about -5 percent at $M_s = 6$. The neglect of the latter contribution appears reasonable for the range of M_s considered herein.

RESULTS AND DISCUSSION

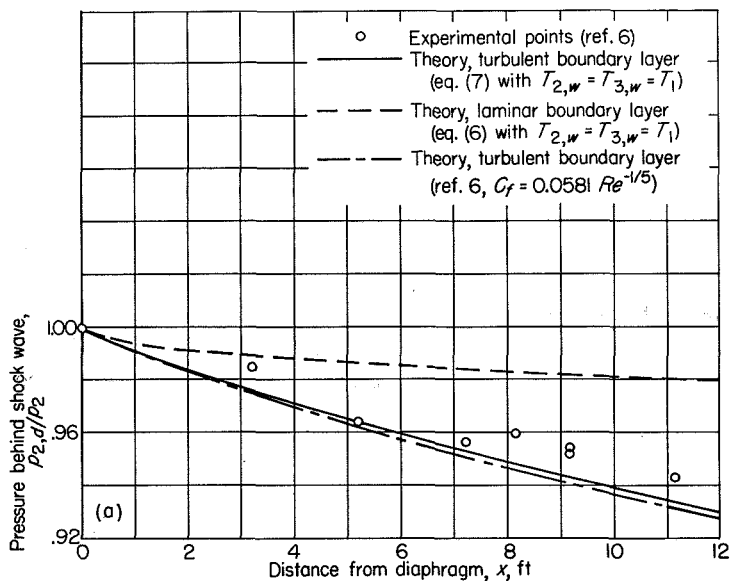
Equations (6) and (7) define the attenuation in a shock tube when the boundary layer is wholly laminar or turbulent, respectively. These equations are now compared with the experimental and theoretical results of reference 6.

COMPARISON WITH EXPERIMENTS OF REFERENCE 6

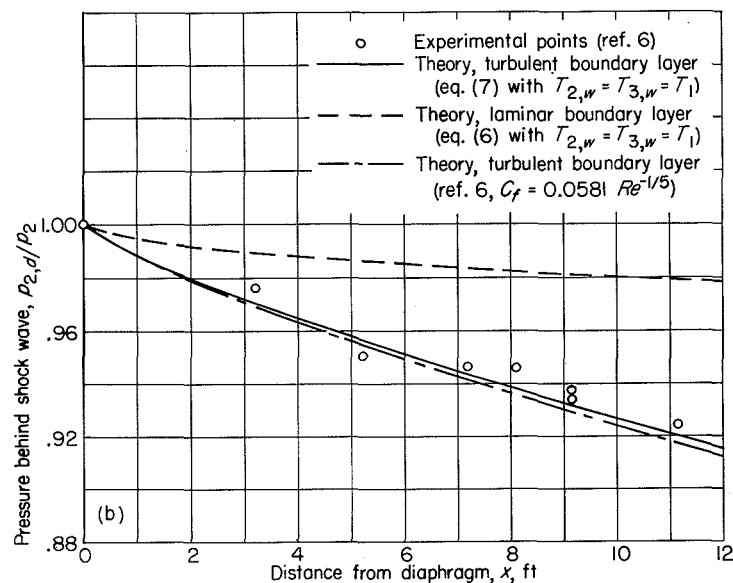
Measurements of shock attenuation were obtained in the investigation of reference 6 by using a high-pressure shock tube having a $\frac{1}{8}$ - by $\frac{1}{8}$ -foot rectangular cross section. Air at room temperature was used in regions 1 and 4. The air in region 1 was maintained at atmospheric pressure. Four

sets of runs, corresponding to $p_4/p_1=4.061, 5.764, 7.455,$ and $17.915,$ are reported. The results of these runs are summarized in figures 7 (a) to (d), respectively. Some of the theoretical curves of reference 6 are included in these figures. The theoretical predictions of equations (6) and (7) are also indicated in figure 7. The latter were found from figure 3 with $p_1=2117,$ and by assuming the wall to be a perfect conductor (since the shock tube had metal walls except for a pair of schlieren glass inserts).

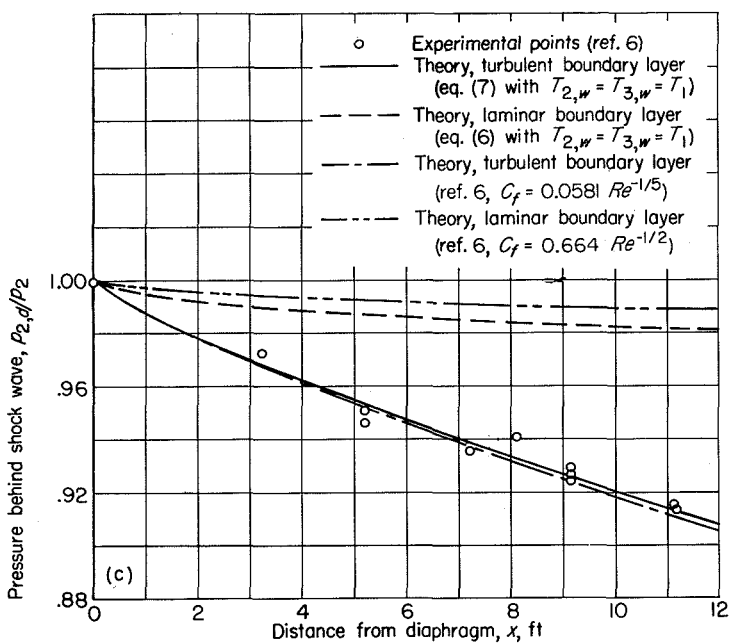
The Reynolds number at the contact surface for these tests is given directly by figure 3. The boundary-layer thickness at point b of region 2 for the test conditions of



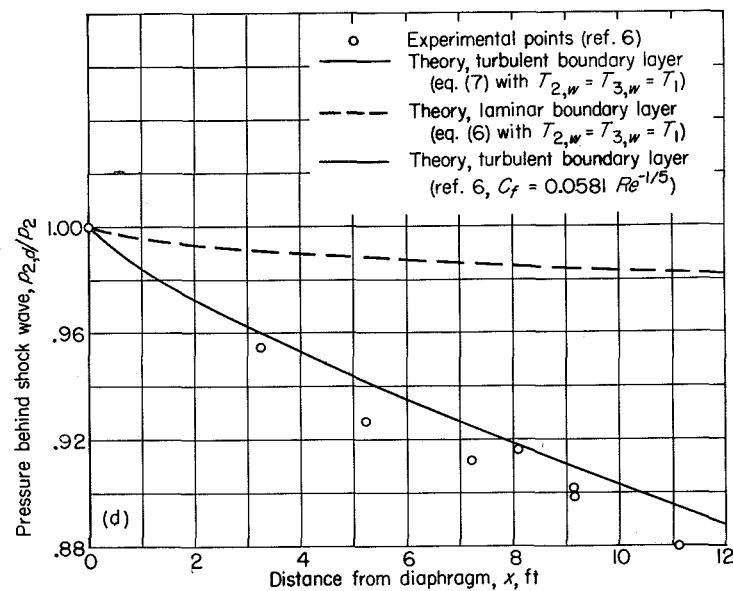
(a) Pressure ratio $p_4/p_1, 4.061$; shock Mach number relative to wall $M_s, 1.344.$



(b) Pressure ratio $p_4/p_1, 5.764$; shock Mach number relative to wall $M_s, 1.442.$



(c) Pressure ratio $p_4/p_1, 7.455$; shock Mach number relative to wall $M_s, 1.518.$



(d) Pressure ratio $p_4/p_1, 17.915$; shock Mach number relative to wall $M_s, 1.792.$

FIGURE 7.—Pressure behind shock wave as function of distance from diaphragm. Air-air shock tube. $T_1=T_4=520^\circ \text{ R}$; hydraulic diameter $d, 1/7.$

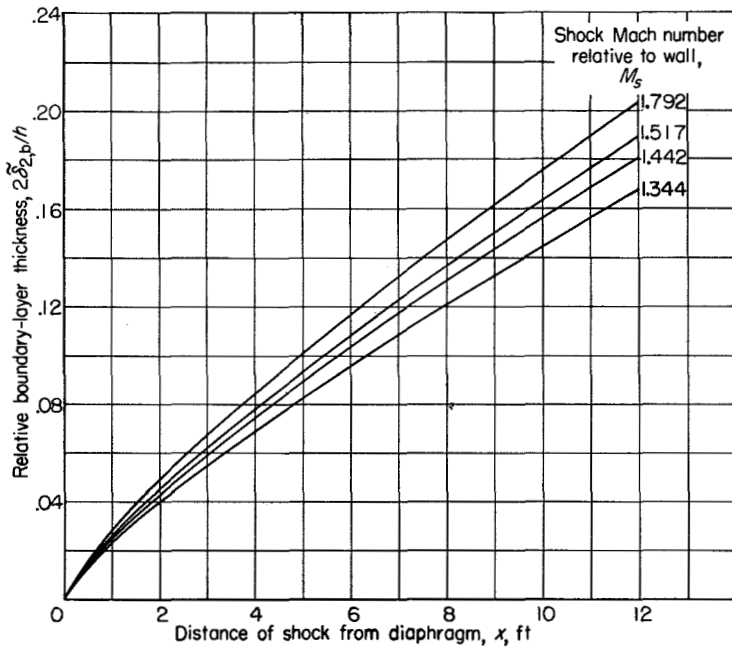


FIGURE 8.—Relative boundary-layer thickness at point b of region 2 for experimental conditions of reference 6 (air in region 1; turbulent boundary layer; $T_1 = T_{2,w} = 520^\circ \text{R}$; h , 1/8 ft).

reference 6 is plotted in figure 8. It is assumed in figure 8 that the boundary layer in region 2 is wholly turbulent and that the wall is a perfect conductor. The boundary-layer thickness is presented in the form of a relative thickness $2\bar{\delta}_{2,b}/h$ where h is the smallest shock-tube dimension normal to the flow and equals $\frac{1}{8}$ for the shock tube of reference 6. When $2\bar{\delta}_{2,b}/h$ is small compared with 1, the assumption of a thin boundary layer is valid, and the theory of the present report is applicable. It may be seen from figure 8 that $2\bar{\delta}_{2,b}/h \leq 0.20$ for $x \leq 12$ for the test conditions of reference 6. Since $2\bar{\delta}_{2,b}/h$ tends to overestimate the effective boundary-layer thickness (because of the asymptotic manner in which the velocities approach free-stream conditions at the edge of the boundary layer),³ figure 8 indicates that the theory of the present report is applicable for comparison with the experiments of reference 6.

In figure 7 (a), the first data point ($x \cong 3'$) is close to the theoretical value for a wholly laminar boundary layer. The other points fall somewhat above the theoretical curve for a wholly turbulent boundary layer. The Reynolds number per foot at the contact surface for this case is $Re_{2,b}/x = 0.4 \times 10^6$ (fig. 3). Using $Re = 0.5 \times 10^6$ as a rough indication of the transition Reynolds number, as discussed in appendix H, it is reasonable to have the first data point near the laminar curve and the other points near the turbulent curve.

The experimental results for $M_s = 1.442$ are given in figure 7 (b). The Reynolds number at the contact surface is

³ A properly computed displacement thickness would probably give a better estimate of the effective boundary-layer thickness.

$Re_{2,b}/x = 0.8 \times 10^6$. The data agree quite well with the values for a wholly turbulent boundary layer. There is a slight tendency for the points to lie above the theoretical curve, which might be attributed to the short length of laminar boundary layer directly behind the shock wave.

The experimental results for $M_s = 1.518$ ($Re_{2,b}/x = 1.1 \times 10^6$) are given in figure 7 (c) and are in excellent agreement with the turbulent-boundary-layer theory of the present report.

In figure 7 (d), the experimental results ($M_s = 1.792$, $Re_{2,b}/x = 2.8 \times 10^6$) fall somewhat below the theoretical predictions of the turbulent-boundary-layer theory of the present report.

In general, the theory seems to agree reasonably well with experiment for the range of data considered in figure 7. Figure 7 (d) indicates the poorest correlation and suggests that the present theory may underestimate the attenuation corresponding to large values of M_s .

COMPARISON WITH THEORY OF REFERENCE 6

The present analysis assumes a relatively thin boundary layer, and the calculations are based on the vertical velocity at the edge of the boundary layer. The numerical value of v depends on terms which are related to the boundary-layer velocity profile, dissipation, and heat transfer. See, for example, equations (D3a) and (D3c). These terms correspond to the use of wall shear, dissipation, and heat transfer in reference 6. Dissipation and heat transfer play similar roles (qualitatively) in the present analysis and in reference 6. However, it can be shown that the velocity-profile term in the equation for v has a sign opposite to that of the wall-shear term in reference 6 for characteristic lines ab and bc (e. g., appendix I). Therefore, the integrations along lines ab and bc , in reference 6, overestimate and underestimate, respectively, the contributions of these characteristic lines to shock attenuation. If the same boundary-layer theory is used, the attenuation calculations of the present report and of reference 6 should be in quantitative agreement only in the limiting case $M_s \rightarrow 1$ (for which the contributions of characteristic lines ab and bc are negligible) and for those values of M_s where the errors due to characteristic lines ab and bc tend to compensate.

Since different boundary-layer theories were used in reference 6 and herein, it is not directly possible to separate the discrepancies between the two methods due to the respective boundary-layer theories from the discrepancies due to basing the attenuation calculations on wall-shear, dissipation, and heat-transfer terms rather than on v . An estimate of the latter discrepancy can be obtained by reversing the sign of the first term in the equations for L_2 (eq. (D3c)) and L_3 (eq. (D4c)) for the integrations of v along characteristic lines bc and ab . Such a procedure shows that the theory of the present report and that of reference 6 agree at $M_s = 1$. With increasing M_s , reference 6 first overestimates the at-

tenuation because of the increasing importance of characteristic line ab . At $M_s=0(1.5)$, reference 6 overestimates attenuation by about 10 to 15 percent. With further increases in M_s , the errors in characteristic line bc become important and tend to compensate for the errors in line ab so that the discrepancy between the two methods decreases. At $M_s=0(2)$, the two methods are again in approximate agreement. As M_s increases further, line ab becomes relatively less important compared with bc , and the theory of reference 6 underestimates the attenuation. At $M_s=6$, the method of reference 6 appears to underestimate the attenuation by about 50 percent. The above figures are only approximate because of the manner in which they were obtained, but they indicate the proper trend with M_s .

From figure 5 (b) it can be seen that the attenuation theory of reference 6 (for turbulent boundary layers) is in good agreement with that of the present report for $1 \leq M_s \leq 2$. The agreement is somewhat better than that to be expected from the discussion of the previous paragraph. Hence, either theory could be used to correlate the experimental data of figure 7. For $M_s > 2$, reference 6 considerably underestimates the attenuation. The laminar-boundary-layer theory of reference 6 differs by a factor of about 2 from that of the present report; therefore, there is a large discrepancy between the theoretical laminar-boundary-layer curves in figure 7 (c).

CONCLUDING REMARKS

A method is presented for computing the attenuation of a shock wave due to unsteady-boundary-layer action. The various assumptions involved in the analysis are summarized in this section, since these define the limitations of the method and suggest possible fields for improvements:

1. Small perturbations: The equations of motion were linearized, assuming the potential flow external to the wall boundary layer undergoes only small perturbations. For long shock tubes with large amounts of attenuation, it might be advisable to employ a characteristic method.

2. Thin boundary layer: The assumption of a thin boundary layer (relative to shock-tube diameter) is consistent with the assumption of small perturbations of the potential flow. If the viscous effects span the entire tube cross section (i. e., long tubes), it may be advisable to base the shock-attenuation theory on wall shear.

3. One-dimensional longitudinal waves: It was previously pointed out that the perturbations in a shock tube should be computed by assuming each element of wall surface area to be an elemental acoustic source of strength proportional to v . This gives rise to a complex wave pattern involving both longitudinal and transverse waves. For the purposes of the present analysis it was assumed that the longitudinal waves are of primary interest and that these can be computed on the basis of a simplified one-dimensional theory. This assumption is accurate when an observer is relatively far

from the sources (since the details of the source distribution around a perimeter then become relatively unimportant) but introduces errors when the observer is near the sources. It would seem that the assumption of one-dimensional longitudinal waves is accurate for weak shocks but introduces errors for stronger shocks, particularly when the flow relative to the wall is supersonic.

4. Boundary-layer theory: The boundary-layer theory of reference 2 was used. It may be assumed that the laminar-boundary-layer solution is reliable except possibly for very strong shock waves. In the latter case, very large temperature gradients exist normal to the wall, and it may be advisable to choose a different reference temperature from that used herein. Also, for strong shock waves, dissociation might occur, which would require changes in the laminar-boundary-layer theory. The turbulent-boundary-layer theory of reference 2 requires experimental verification for even the weak-shock case. However, the good agreement between the attenuation calculation based on the turbulent boundary layer of reference 2 and the experiments of reference 6 suggests that the turbulent-boundary-layer theory of reference 2 gives reasonable results, at least for the weak-shock case.

5. Expansion wave of zero thickness: In order to simplify the problem of determining the boundary layer behind an expansion wave, it was assumed in reference 2 that the expansion wave is of negligible thickness (i. e., "expansion shock"). This assumption is valid for weak expansion waves but is in error for strong expansion waves. The boundary-layer solution for region 3 might be improved for the strong-wave case by considering the finite thickness of the expansion wave. However, the contribution to shock attenuation of region 3 becomes small for the strong-wave case, so that an improved boundary-layer solution for region 3 may not significantly affect the attenuation calculation.

In addition to the preceding discussion, the following extensions of the present report might be pursued:

1. The details for obtaining the perturbations at a fixed point in the shock tube, as opposed to finding the shock attenuation as is done herein, might be treated. This would be useful for further correlating the theory with experiment and for determining conditions at an aerodynamic model (when the shock tube is used as a wind tunnel).

2. Formulas equivalent to equations (6) and (7) might be derived for the case where the boundary layer is partly laminar and partly turbulent.

3. The boundary-layer theory as outlined in appendixes D and E might be simplified, particularly for the turbulent case, so as to give reasonably accurate results without too tedious a boundary-layer calculation.

LEWIS FLIGHT PROPULSION LABORATORY

NATIONAL ADVISORY COMMITTEE FOR AERONAUTICS

CLEVELAND, OHIO, April 24, 1956

APPENDIX A

SYMBOLS

The following symbols are used in this report:

A	cross-sectional area of tube
a	speed of sound
C	eq. (C3)
c_p	specific heat at constant pressure
c_v	specific heat at constant volume
D	eq. (C3)
d	hydraulic diameter, $4A/l$
E	eq. (C7)
F	eq. (C7)
h	smallest shock-tube dimension normal to flow
k	thermal conductivity
L_2, L_3	appendixes D and E
l	perimeter of shock-tube cross section
M	Mach number of flow relative to wall
M_s	shock Mach number relative to wall
M_2, M_3	Mach number of flow in regions 2 and 3, relative to wall
m	rate of mass addition per unit cross-sectional area per unit x
n_2, n_3	appendixes D and E
p	pressure, lb/sq ft
Re	Reynolds number (appendix H)
$Re_{2,b}$	Reynolds number at point b of region 2,

$$\frac{a_1 x}{\nu_1} \left[\nu_{12} \left(\frac{u_2}{u_s} \right)^2 \left(1 + M_2 - \frac{u_s}{a_2} \right) M_s \right], \text{ appendix H}$$

T	temperature, °R
T_w	temperature of insulated wall
t	time
u	velocity of flow relative to wall

u_s	velocity of shock wave relative to wall
u_2, u_3	velocity in regions 2 and 3 relative to wall
v	vertical velocity (positive when directed into tube) at edge of boundary layer
x	longitudinal distance
γ	ratio of specific heats
Δ	perturbation quantity (Δp = perturbation of p , etc.)
δ_2	laminar-boundary-layer thickness in region 2 (eq. (D5))
$\tilde{\delta}_2$	turbulent-boundary-layer thickness in region 2 (eq. (E3))
μ	coefficient of viscosity
ν	kinematic viscosity
ξ	integration variable representing x
ρ	mass density
σ	Prandtl number
τ	integration variable representing t

Subscripts:

1, 2, 3, 4	regions of shock tube (fig. 1)
a, b, c, d, e	points on characteristic lines (fig. 2)
m	evaluated at mean temperature of boundary layer (appendixes D and E)
w	evaluated at wall

Superscripts:

+	associated with wave moving downstream (+ x -direction)
-	associated with wave moving upstream (- x -direction)

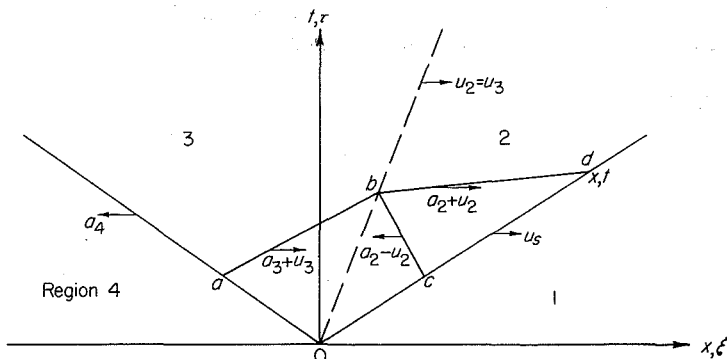
Special notation:

$a_{32} \equiv a_3/a_2$; $p_{12} \equiv p_1/p_2$, etc. (Two successive integer subscripts, not separated by a comma, represent a ratio.)

APPENDIX B

CHARACTERISTIC-LINE GEOMETRY AND SOME INTEGRALS

The equations of the characteristic lines considered in the present report are summarized. Some important integrals are indicated. It is assumed that the characteristic lines are straight (corresponding to the ideal-flow case) and that the expansion fan can be considered as an "expansion shock" (i. e., expansion wave of zero thickness) moving with velocity a_4 into region 4 (following sketch). The point d with coordinates x, t is assumed to be on the shock-wave characteristic.



The equations of the characteristic lines are

Line bd :

$$\xi = x - (a_2 + u_2)(t - \tau)$$

$$\tau = t - \frac{x - \xi}{a_2 + u_2}$$

$$u_s \tau - \xi = \left[\frac{1 + M_2 - (u_s/a_2)}{1 + M_2} \right] (x - \xi)$$

Line ab :

$$\xi = \xi_b - (a_3 + u_3)(\tau_b - \tau)$$

$$\tau = \tau_b - \frac{\xi_b - \xi}{a_3 + u_3}$$

$$a_4 \tau + \xi = \left(\frac{1 + M_3 + a_{43}}{1 + M_3} \right) (\xi - \xi_a)$$

Line bc :

$$\xi = \xi_b + (a_2 - u_2)(\tau_b - \tau)$$

$$\tau = \tau_b - \frac{\xi - \xi_b}{a_2 - u_2}$$

$$u_s \tau - \xi = \left[\frac{1 - M_2 + (u_s/a_2)}{1 - M_2} \right] (\xi_c - \xi)$$

(B1)

In terms of x, t , the coordinates of points a , b , and c are

$$\left. \begin{aligned} \text{Point } a: \quad & \xi_a = -x \left[\frac{1+M_2 - (u_s/a_2)}{1+M_3 + a_{43}} \right] \frac{a_4}{u_s} \\ & \tau_a = t \left[\frac{1+M_2 - (u_s/a_2)}{1+M_3 + a_{43}} \right] \\ \text{Point } b: \quad & \xi_b = x[1+M_2 - (u_s/a_2)] \frac{u_2}{u_s} \\ & \tau_b = t[1+M_2 - (u_s/a_2)] \\ \text{Point } c: \quad & \xi_c = x \left[\frac{1+M_2 - (u_s/a_2)}{1-M_2 + (u_s/a_2)} \right] \\ & \tau_c = t \left[\frac{1+M_2 - (u_s/a_2)}{1-M_2 + (u_s/a_2)} \right] \end{aligned} \right\} \quad (\text{B2})$$

Some important line integrals are

$$\left. \begin{aligned} \frac{1}{1+M_2} \int_{\xi_b}^x (u_s \tau - \xi)^{-n_2} d\xi &= (1-u_2/u_s)^{1-n_2} \left(1+M_2 - \frac{u_s}{a_2}\right)^{-n_2} \left(\frac{x^{1-n_2}}{1-n_2}\right) \\ \frac{1}{1-M_2} \int_{\xi_b}^{\xi_c} (u_s \tau - \xi)^{-n_2} d\xi &= \frac{\xi_c}{x} \left[\left(1 - \frac{u_2}{u_s}\right)^{1-n_2} \left(1+M_2 - \frac{u_s}{a_2}\right)^{-n_2} \left(\frac{x^{1-n_2}}{1-n_2}\right) \right] \\ \frac{1}{1+M_3} \int_{\xi_a}^{\xi_b} (a_4 \tau + \xi)^{-n_3} d\xi &= (1+u_3/a_4)^{1-n_3} \frac{\left[\left(1+M_2 - \frac{u_s}{a_2}\right) \frac{a_4}{u_s} \right]^{1-n_3}}{1+M_3 + a_{43}} \left(\frac{x^{1-n_3}}{1-n_3}\right) \end{aligned} \right\} \quad (\text{B3})$$

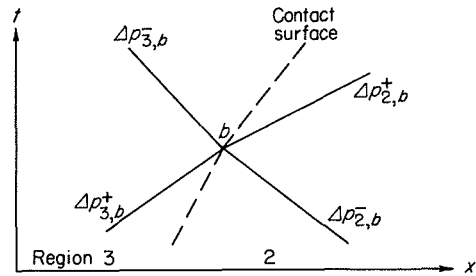
APPENDIX C

INTERACTION OF PRESSURE WAVES WITH INTERFACES

Weak pressure waves are assumed to overtake a contact surface or a shock wave. The strength of the reflected and transmitted waves is found.

CONTACT SURFACE

Consider the contact surface which separates region 3 from region 2 (following sketch). At a certain instant, known



incident waves $\Delta p_{3,b}^+$ and $\Delta p_{2,b}^-$ intersect the surface. The problem is to find the final waves $\Delta p_{3,b}^-$ and $\Delta p_{2,b}^+$. From isentropic flow relations,

$$\left. \begin{aligned} \Delta p^+ &= \rho a \Delta u^+ \\ \Delta p^- &= -\rho a \Delta u^- \end{aligned} \right\} \quad (\text{C1})$$

The boundary conditions across the contact surface are

$$\left. \begin{aligned} \Delta u_{2,b}^+ + \Delta u_{2,b}^- &= \Delta u_{3,b}^+ + \Delta u_{3,b}^- \\ \Delta p_{2,b}^+ + \Delta p_{2,b}^- &= \Delta p_{3,b}^+ + \Delta p_{3,b}^- \end{aligned} \right\} \quad (\text{C2})$$

From equations (C1) and (C2), the expressions for $\Delta p_{2,b}^+$ and $\Delta p_{3,b}^-$ are

$$\left. \begin{aligned} \Delta p_{2,b}^+ &= C \Delta p_{2,b}^- + D \Delta p_{3,b}^+ \\ \Delta p_{3,b}^- &= \gamma_{32} a_{23} D \Delta p_{2,b}^- - C \Delta p_{3,b}^+ \end{aligned} \right\} \quad (\text{C3})$$

where

$$C \equiv (\gamma_{32} a_{23} - 1) / (\gamma_{32} a_{23} + 1)$$

$$D \equiv 2 / (\gamma_{32} a_{23} + 1)$$

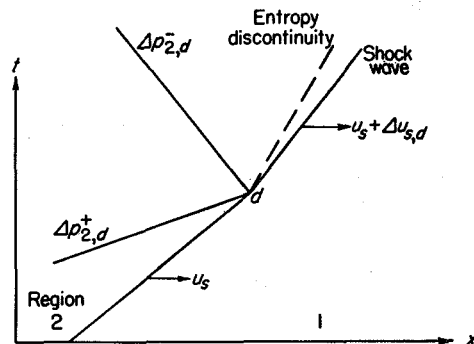
The quantities C and D are reflection and transmission coefficients, respectively.

SHOCK WAVE

Consider a shock wave moving with velocity u_s into a stationary fluid (region 1). The region behind the shock is designated as region 2. Conditions in regions 1 and 2 can be found from shock-wave theory. In particular, with $\gamma_1 = \gamma_2$,

$$\left. \begin{aligned} p_{21} &= \frac{2\gamma_1 M_s^2 - (\gamma_1 - 1)}{\gamma_1 + 1} \\ \frac{u_2}{a_1} &= \frac{2}{\gamma_1 + 1} \left(M_s - \frac{1}{M_s} \right) \\ \rho_{21} &= \frac{(\gamma_1 + 1) M_s^2}{(\gamma_1 - 1) M_s^2 + 2} \end{aligned} \right\} \quad (\text{C4})$$

At a certain instant, a known wave $\Delta p_{2,d}^+$ intersects the shock (following sketch).



The problem is to determine the net perturbation of the shock wave. From equations (C4),

$$\left. \begin{aligned} \frac{\Delta p_{2,a}}{p_2} &= \frac{4\gamma_1}{\gamma_1+1} p_{12} M_s \Delta M_{s,a} \\ \frac{\Delta u_{2,a}}{a_1} &= \frac{2}{\gamma_1+1} \left(1 + \frac{1}{M_s^2}\right) \Delta M_{s,a} \\ \frac{\Delta \rho_{2,a}}{\rho_2} &= \frac{4}{(\gamma_1-1)M_s^2+2} \frac{\Delta M_{s,a}}{M_s} \end{aligned} \right\} \quad (C5)$$

The net pressure and velocity perturbations in region 2 are then related by

$$\Delta p_{2,a} = 2\rho_1 a_1 \frac{M_s^3}{1+M_s^2} \Delta u_{2,a} \quad (C6)$$

With $\Delta p_{2,a} \equiv \Delta p_{2,a}^+ + \Delta p_{2,a}^-$ and $\Delta u_{2,a} \equiv \Delta u_{2,a}^+ + \Delta u_{2,a}^-$, using equations (C1) gives

$$\left. \begin{aligned} \Delta p_{2,a}^- &= E \Delta p_{2,a}^+ \\ \Delta p_{2,a} &= F \Delta p_{2,a}^+ \end{aligned} \right\} \quad (C7)$$

where

$$E \equiv \left(2\rho_{12} a_{12} \frac{M_s^3}{1+M_s^2} - 1 \right) / \left(2\rho_{12} a_{12} \frac{M_s^3}{1+M_s^2} + 1 \right)$$

$$F \equiv \left(4\rho_{12} a_{12} \frac{M_s^3}{1+M_s^2} \right) / \left(2\rho_{12} a_{12} \frac{M_s^3}{1+M_s^2} + 1 \right)$$

The quantity E is a reflection coefficient. The resulting perturbation of the shock Mach number is

$$\frac{\Delta M_{s,a}}{M_s} = \frac{\gamma_1+1}{4\gamma_1} \frac{p_{21}}{M_s^2} F \frac{\Delta p_{2,a}^+}{p_2} \quad (C8)$$

For $M_s=1$, $\frac{\Delta p_{2,a}^-}{\Delta p_{2,a}^+} = 0$. For M_s infinitely large,

$$\frac{\Delta p_{2,a}^-}{\Delta p_{2,a}^+} = \frac{2\sqrt{\frac{\gamma_1-1}{2\gamma_1}} - 1}{2\sqrt{\frac{\gamma_1-1}{2\gamma_1}} + 1}$$

which becomes $\frac{\Delta p_{2,a}^-}{\Delta p_{2,a}^+} = -0.14$ for $\gamma_1=1.4$, indicating that the reflected wave is relatively small and is opposite in sign to the incident wave.

APPENDIX D

LAMINAR BOUNDARY LAYER BEHIND WAVE

The laminar boundary layer behind a shock or thin expansion wave is analyzed in reference 2. Some of the results are summarized herein. It is assumed that the wall temperature behind the wave is constant and that σ and c_p are independent of temperature. The fluid properties μ and k are referenced to a mean temperature as discussed in appendix C of reference 2. The notation of reference 2 is compared with the notation of the present report in the following equations. The left side of each equation represents the notation of reference 2, while the right side is in the notation of the present report.

Region 2

$$\left. \begin{aligned} u_w &= u_s & \frac{u_w}{u_e} &= \frac{1}{1-(u_2/u_s)} \\ u_e &= u_s - u_2 & & \\ v_e &= v_2 & \frac{u_w}{u_e} - 1 &= \frac{u_2/u_s}{1-(u_2/u_s)} \\ x &= u_s \tau - \xi & & \end{aligned} \right\} \quad (D1)$$

Region 3

$$\left. \begin{aligned} u_w &= a_4 & \frac{u_w}{u_e} &= \frac{1}{1+(u_3/a_4)} \\ u_e &= a_4 + u_3 & & \\ v_e &= v_3 & \frac{u_w}{u_e} - 1 &= \frac{-u_3/a_4}{1+(u_3/a_4)} \\ x &= a_4 \tau + \xi & & \end{aligned} \right\} \quad (D2)$$

VERTICAL VELOCITY AT EDGE OF BOUNDARY LAYER

The expression for the vertical velocity at the edge of the boundary layer can now be written as follows:

Region 2

$$v_2 = -L_2 \left[\frac{u_2^2/u_s}{1-(u_2/u_s)} \right]^{1-n_2} \left(\frac{v_2}{u_s \tau - \xi} \right)^{n_2} \quad (D3a)$$

where

$$n_2 = \frac{1}{2} \quad (D3b)$$

$$L_2 = \sqrt{\frac{1}{2} \frac{\mu_{2,m}}{\mu_2} \frac{T_2}{T_{2,m}}} \left\{ \lim_{\eta \rightarrow \infty} \left[\frac{(f-\eta) \left(1 - \frac{u_2}{u_s}\right)}{u_2/u_s} \right] - \frac{\gamma_2-1}{2} M_2 \left(\frac{u_s}{a_2}\right) \left(1 - \frac{u_2}{u_s}\right) \int_0^\infty r_2 d\eta + \frac{1-(u_2/u_s)}{(u_2/u_s)} \left(\frac{T_{2,r}}{T_2} - \frac{T_{2,w}}{T_2}\right) \int_0^\infty s_2 d\eta \right\} \quad (D3c)$$

$$\lim_{\eta \rightarrow \infty} \left[\frac{(f-\eta) \left(1 - \frac{u_2}{u_s}\right)}{u_2/u_s} \right] = 1.134 \sqrt{\frac{1-(u_2/u_s)}{2.022-(u_2/u_s)}} \quad (D3d)$$

$$\int_0^\infty r_2 d\eta = 1.569 \sqrt{\frac{1-(u_2/u_s)}{1.933-(u_2/u_s)}} (\sigma_2)^{\frac{-0.045u_2/u_s}{1-(u_2/u_s)}} \quad (D3e)$$

$$\int_0^\infty s_2 d\eta = 1.134 \sqrt{\frac{1-(u_2/u_s)}{2.022-(u_2/u_s)}} (\sigma_2)^{\frac{-0.50+0.47(u_2/u_s)}{1-(u_2/u_s)}} \quad (D3f)$$

$$r_2(0) = (\sigma_2)^{\frac{0.37-0.39(u_2/u_s)}{1-(u_2/u_s)}} \quad (D3g)$$

$$\frac{T_{2,r}}{T_2} = 1 + \frac{\gamma_2-1}{2} M_2^2 r_2(0) \quad (D3h)$$

$$\frac{\rho_2}{\rho_{2,m}} = \frac{T_{2,m}}{T_2} = 0.5 \left(\frac{T_{2,w}}{T_2} + 1 \right) + 0.22 \left(\frac{T_{2,r}}{T_2} - 1 \right) \quad (D3i)$$

The above quantities can be evaluated if the wall surface temperature $T_{2,w}$ is known. The value of $T_{2,w}$ depends on the heat capacity and conduction properties of the wall and the wall thickness. A method for evaluating $T_{2,w}$ is presented in reference 2. From the discussion in reference 2, it may be concluded that in most cases $T_{2,w}$ approximately equals T_1 when the wall is a metal.

Region 3

$$v_3 = L_3 \left(\frac{u_3^2/a_4}{1+u_3/a_4} \right)^{1-n_3} \left(\frac{v_3}{a_4\tau+\xi} \right)^{n_3} \quad (\text{D4a})$$

where

$$n_3 = 1/2 \quad (\text{D4b})$$

$$L_3 = \sqrt{\frac{1}{2} \frac{\mu_{3,m}}{\mu_3} \frac{T_3}{T_{3,m}}} \left\{ \lim_{\eta \rightarrow \infty} \left[\frac{(\eta-f)(1+u_3/a_4)}{u_3/a_4} \right] + \frac{\gamma_3-1}{2} M_3 a_{43} \left(1 + \frac{u_3}{a_4} \right) \int_0^\infty r_3 d\eta + \frac{1+(u_3/a_4)}{u_3/a_4} \left(\frac{T_{3,w}}{T_3} - \frac{T_{3,r}}{T_3} \right) \int_0^\infty s_3 d\eta \right\} \quad (\text{D4c})$$

$$\lim_{\eta \rightarrow \infty} \left[\frac{(\eta-f)(1+u_3/a_4)}{u_3/a_4} \right] = 1.217 \sqrt{\frac{1+(u_3/a_4)}{2.326+(u_3/a_4)}} \quad (\text{D4d})$$

$$\int_0^\infty r_3 d\eta = 1.686 \sqrt{\frac{1+(u_3/a_4)}{2.234+(u_3/a_4)}} (\sigma_3)^{\frac{0.22u_3/a_4}{1+(u_3/a_4)}} \quad (\text{D4e})$$

$$\int_0^\infty s_3 d\eta = 1.217 \sqrt{\frac{1+(u_3/a_4)}{2.326+(u_3/a_4)}} (\sigma_3)^{\frac{-0.50-0.36(u_3/a_4)}{1+(u_3/a_4)}} \quad (\text{D4f})$$

$$r_3(0) = (\sigma_3)^{\frac{0.37+0.50(u_3/a_4)}{1+(u_3/a_4)}} \quad (\text{D4g})$$

$$\frac{T_{3,r}}{T_3} = 1 + \frac{\gamma_3-1}{2} M_3^2 r_3(0) \quad (\text{D4h})$$

$$\frac{T_{3,m}}{T_3} = 0.5 \left(\frac{T_{3,w}}{T_3} + 1 \right) + 0.22 \left(\frac{T_{3,r}}{T_3} - 1 \right) \quad (\text{D4i})$$

Equations (D4) can be evaluated if $T_{3,w}$ is known. If the wall is initially at temperature T_4 , then $T_{3,w} = T_4$ is generally a good estimate for $T_{3,w}$, as is discussed in reference 2.

BOUNDARY-LAYER THICKNESS IN REGION 2

In the body of the report it is assumed that the boundary layer is thin relative to the shock-tube diameter. It is therefore of interest to present an expression defining boundary-layer thickness. Region 2 is of particular interest since the boundary layer in region 2 is generally larger than that in region 3. Let δ_2 represent the laminar-boundary-layer thickness in region 2, defined so as to correspond to $\frac{u}{u_2} = 0.99$. From equation (18) of reference 3,

$$\delta_2 = \sqrt{\frac{2}{1-\frac{u_2}{u_s}}} \sqrt{\frac{\mu_{2,m} T_2}{\mu_2 T_{2,m}}} \sqrt{\frac{v_2(u_s\tau-\xi)}{u_s}} \left[\frac{2.89 \sqrt{1-u_2/u_s}}{\sqrt{1.413-u_2/u_s}} + \frac{\gamma_2-1}{2} M_2^2 \int_0^\infty r_2 d\eta - \left(\frac{T_{2,r}}{T_2} - \frac{T_{2,w}}{T_2} \right) \int_0^\infty s_2 d\eta \right] \quad (\text{D5})$$

(Eq. (D5) uses a mean reference temperature and an interpolation formula for η_s (defined in ref. 3) and takes the upper limit on the integrals to be ∞ rather than η_s .) To evaluate δ_2 along the characteristic line bd of figure 2, take $u_s\tau - \xi$ equal to $\left(\frac{1+M_2-u_s/a_2}{1+M_2} \right) (x-\xi)$. The value of δ_2 at point b is found by replacing $u_s\tau - \xi$ by $\left(\frac{1+M_2-u_s/a_2}{1+M_2} \right) \left(1 - \frac{u_2}{u_s} \right) x$.

APPENDIX E

TURBULENT BOUNDARY LAYER BEHIND WAVE

The turbulent boundary layer behind a shock or thin expansion wave is also studied in reference 2 for the case of constant wall surface temperature. The correspondence between the notation of reference 2 and that of the present report was previously noted in equations (D1) and (D2). The turbulent-boundary-layer solution of reference 2 (relating to v) is now summarized. It is assumed that the wall surface temperature is essentially constant.

VERTICAL VELOCITY AT EDGE OF BOUNDARY LAYER

Region 2

$$v_2 = -L_2 \left[\frac{u_2^2/u_s}{1-(u_2/u_s)} \right]^{1-n_2} \left(\frac{v_2}{u_s\tau-\xi} \right)^{n_2} \quad (\text{E1a})$$

where

$$n_2 = 1/5 \quad (\text{E1b})$$

$$L_2 = 0.0460 \frac{\delta_2^* [(u_2/u_s) - 1]}{\delta_2 [(u_2/u_s)]} \left\{ \varphi_2 \frac{\tilde{\delta}_2 (u_2/u_s)}{\theta_2 [(u_2/u_s) - 1]} \right\}^{1/5} \quad (\text{E1c})$$

$$\frac{\delta_2^* (u_2/u_s) - 1}{\delta_2 (u_2/u_s)} = \frac{u_s}{u_2} \left[\left(\frac{T_2}{T_{2,w}} + \frac{u_2}{u_s} - 1 \right) \left(1 - 7 \frac{T_2}{T_{2,w}} I_{2,7} \right) - 7c_2 \frac{T_2}{T_{2,w}} (I_{2,7} - I_{2,8}) \right] \quad (\text{E1d})$$

$$\frac{\theta_2 (u_2/u_s) - 1}{\delta_2 (u_2/u_s)} = \frac{T_2/T_{2,w}}{1-(u_2/u_s)} \left[\left(1 - 7 \frac{T_2}{T_{2,w}} I_{2,7} \right) - \right.$$

$$\left. 7 \left(c_2 + \frac{u_2}{u_s} \right) (I_{2,7} - I_{2,8}) \right] \quad (\text{E1e})$$

$$\varphi_2 = \left(\frac{\mu_{2,m}}{\mu_2} \right)^{1/4} \left(\frac{T_2}{T_{2,m}} \right)^{3/4} \quad (\text{E1f})$$

$$I_{2,N} = \int_0^1 \frac{z^N dz}{1+b_2 z - c_2 z^2} \quad (\text{E1g})$$

$$b_2 = \frac{T_{2,r}}{T_{2,w}} - 1 \quad (\text{E1h})$$

$$c_2 = \left(\frac{T_{2,r}}{T_2} - 1 \right) \left(\frac{T_2}{T_{2,w}} \right) \quad (\text{E1i})$$

$$\frac{T_{2,r}}{T_2} = 1 + \frac{\gamma_2-1}{2} M_2^2 (\sigma_2)^{1/5} \quad (\text{E1j})$$

$$\frac{T_{2,m}}{T_2} = 0.5 \left(\frac{T_{2,w}}{T_2} + 1 \right) + 0.22 \left(\frac{T_{2,r}}{T_2} - 1 \right) \quad (\text{E1k})$$

The conditions under which $T_{2,w}$ essentially equals T_1 can be established by the methods of reference 2. The assumption of $T_{2,w} = T_1$ appears reasonable for most cases.

The integrals $I_{2,7}$ and $I_{2,7} - I_{2,8}$ can be evaluated using table I. Reciprocals are tabulated therein so that linear interpolation is accurate except for b_2 near -1 or $c_2/(b_2+1)$ near 1 . The integrals can be evaluated analytically from the following expressions:

$$\left. \begin{aligned} I_{2,7} &= \frac{1}{\sqrt{b_2^2 + 4c_2}} [(I_{2,7})_{\beta_2} - (I_{2,7})_{\lambda_2}] \\ I_{2,7} - I_{2,8} &= \frac{1}{\sqrt{b_2^2 + 4c_2}} [(\lambda_2 - 1)(I_{2,7})_{\lambda_2} - (\beta_2 - 1)(I_{2,7})_{\beta_2}] \end{aligned} \right\} \quad (\text{E1l})$$

where

$$\lambda_2 = \frac{1}{2c_2} (b_2 + \sqrt{b_2^2 + 4c_2}) \quad (\text{E1m})$$

$$\beta_2 = \frac{1}{2c_2} (b_2 - \sqrt{b_2^2 + 4c_2}) \quad (\text{E1n})$$

$$(I_{2,7})_{\beta_2} = \beta_2^7 \left[\ln \left(\frac{\beta_2 - 1}{\beta_2} \right) + \sum_{m=1}^7 \frac{1}{m} \left(\frac{1}{\beta_2} \right)^m \right] \quad (\text{E1o})$$

$$(I_{2,7})_{\lambda_2} = \lambda_2^7 \left[\ln \left(\frac{\lambda_2 - 1}{\lambda_2} \right) + \sum_{m=1}^7 \frac{1}{m} \left(\frac{1}{\lambda_2} \right)^m \right] \quad (\text{E1p})$$

It can be shown that $\beta_2 < 0$, $\lambda_2 > 1$. Equations (E1o) and (E1p) give accurate results for $-1.6 \leq \beta_2 < 0$ and $1 < \lambda_2 \leq 2$, respectively. For values of β_2 and λ_2 outside these ranges, the right sides of equations (E1o) and (E1p) become the difference of two nearly equal numbers and the following expansions are useful:

$$(I_{2,7})_{\beta_2} = \frac{1}{8(1-\beta_2)} \left[1 + \sum_{m=1}^{\infty} \frac{8!m!}{(8+m)!} \left(\frac{1}{1-\beta_2} \right)^m \right] \quad (\text{E1q})$$

$$(I_{2,7})_{\lambda_2} = \frac{1}{8(1-\lambda_2)} \left[1 - 8 \sum_{m=1}^{\infty} \frac{1}{(7+m)(8+m)} \left(\frac{1}{\lambda_2} \right)^m \right] \quad (\text{E1r})$$

Region 3

$$v_3 = L_3 \left[\frac{u_3^2/a_4}{1 + (u_3/a_4)} \right]^{1-n_3} \left(\frac{v_3}{a_4\tau + \xi} \right)^{n_3} \quad (\text{E2a})$$

where

$$n_3 = \frac{1}{5} \quad (\text{E2b})$$

$$L_3 = 0.0460 \frac{\delta_3^* [1 + (u_3/a_4)]}{\delta_3 (u_3/a_4)} \left\{ \varphi_3 \frac{\delta_3 (u_3/a_4)}{\theta_3 [1 + (u_3/a_4)]} \right\}^{1/5} \quad (\text{E2c})$$

$$\frac{\delta_3^*}{\delta_3} \frac{1 + (u_3/a_4)}{u_3/a_4} = \frac{a_4}{u_3} \left[7c_3 \frac{T_3}{T_{3,w}} (I_{3,7} - I_{3,8}) - \left(\frac{T_3}{T_{3,w}} - \frac{u_3}{a_4} - 1 \right) \left(1 - 7 \frac{T_3}{T_{3,w}} I_{3,7} \right) \right] \quad (\text{E2d})$$

$$\frac{\theta_3}{\delta_3} \frac{1 + (u_3/a_4)}{u_3/a_4} = \frac{T_3/T_{3,w}}{1 + u_3/a_4} \left[\left(1 - 7 \frac{T_3}{T_{3,w}} I_{3,7} \right) - 7 \left(c_3 - \frac{u_3}{a_4} \right) (I_{3,7} - I_{3,8}) \right] \quad (\text{E2e})$$

$$\varphi_3 = \left(\frac{\mu_{3,m}}{\mu_3} \right)^{1/4} \left(\frac{T_3}{T_{3,m}} \right)^{3/4} \quad (\text{E2f})$$

$$I_{3,N} = \int_0^1 \frac{z^N dz}{1 + b_3 z - c_3 z^2} \quad (\text{E2g})$$

$$b_3 = (T_{3,r}/T_{3,w}) - 1 \quad (\text{E2h})$$

$$c_3 = [(T_{3,r}/T_3) - 1] (T_3/T_{3,w}) \quad (\text{E2i})$$

$$\frac{T_{3,r}}{T_3} = 1 + \frac{\gamma_3 - 1}{2} M_3^2 (\sigma_3)^{1/2} \quad (\text{E2j})$$

$$\frac{T_{3,m}}{T_3} = 0.5 \left(\frac{T_{3,w}}{T_3} + 1 \right) + 0.22 \left(\frac{T_{3,r}}{T_3} - 1 \right) \quad (\text{E2k})$$

The conditions under which $T_{3,w}$ essentially equals T_4 can be established by the methods of reference 2. The assumption $T_{3,w} = T_4$ appears reasonable for most cases. The integrals $I_{3,7}$ and $I_{3,7} - I_{3,8}$ can be evaluated using table I or equations (E1l) to (E1r) (with the subscript 2 replaced by the subscript 3 therein).

BOUNDARY-LAYER THICKNESS IN REGION 2

The symbol $\tilde{\delta}_2$ represents the turbulent-boundary-layer thickness as obtained from an integral (Kármán-Pohlhausen) type of boundary-layer solution. From reference 2, it can be shown that

$$\tilde{\delta}_2 = 0.0574 \left\{ \varphi_2 \left[\frac{u_2/u_s}{\frac{\theta_2}{\tilde{\delta}_2} \left(\frac{u_2}{u_s} - 1 \right)} \right] \right\}^{1/4} \frac{(u_2/u_s)^{3/5} \left(\frac{v_2}{u_s} \right)^{1/5} (u_s \tau - \xi)^{1/5}}{(1 - u_2/u_s)^{1/5} \left(\frac{v_2}{u_s} \right)^{1/5}} \quad (\text{E3})$$

The value of $\tilde{\delta}_2$ along characteristic line bd or at point b may be obtained by the substitutions indicated after equation (D5).

APPENDIX F

DEVELOPMENT OF ATTENUATION FORMULAS

The attenuation of the shock wave in a shock tube is now derived. The flow is considered to consist of the ideal shock-tube flow plus small perturbations due to the boundary layer. The ideal flow is uniform in regions 1, 2, 3, and 4, and is denoted by the appropriate subscripts (i. e., p_1, p_2, p_3 , etc.). Perturbations at any point are denoted by Δ and an additional subscript indicating the point. Thus, the perturbations at point b of figure 2 evaluated on the right side of the entropy discontinuity are designated by $\Delta p_{2,b}$, $\Delta u_{2,b}$, and so forth. The expansion wave of the ideal flow is assumed to have negligible thickness and to propagate into region 4 with the velocity $u = -a_4$ as indicated in figure 2.

(The same assumption was used in the attenuation study of ref. 6.)

Let point d of figure 2 represent an arbitrary point on the shock wave. The problem is to find the net pressure perturbation behind the shock (i. e., $\Delta p_{2,d}$). This requires an integration of equation (4) along all characteristic lines which contribute to $\Delta p_{2,d}$. Because of the entropy discontinuities, there are an infinite number of line segments along which the integration must be conducted (fig. 2). However, the major contributions to $\Delta p_{2,d}$ can be shown to come from segments ab , cb , and bd .

If $\Delta p_{2,a}^+$ represents the incident pressure wave at point d , then equation (C7) gives

$$\Delta p_{2,a} = F \Delta p_{2,a}^+ \quad (\text{F1})$$

But, from equation (4),

$$\Delta p_{2,a}^+ = \Delta p_{2,b}^+ + \frac{2\gamma_2 p_2}{a_2 d (1+M_2)} \int_{\xi_b}^x v_2(\xi, \tau) d\xi \quad (\text{F2})$$

where the integration is conducted along the line bd . From equation (C3),

$$\Delta p_{2,b}^+ = C \Delta p_{2,b}^- + D \Delta p_{3,b}^+ \quad (\text{F3})$$

Again, from equation (4),

$$\left. \begin{aligned} \Delta p_{2,b}^- &= \Delta p_{2,c}^- + \frac{2\gamma_2 p_2}{a_2 d (1-M_2)} \int_{\xi_b}^{\xi_c} v_2(\xi, \tau) d\xi \\ \Delta p_{3,b}^+ &= \Delta p_{3,a}^+ + \frac{2\gamma_3 p_3}{a_3 d (1+M_3)} \int_{\xi_a}^{\xi_b} v_3(\xi, \tau) d\xi \end{aligned} \right\} \quad (\text{F4})$$

$$\left(\frac{u_s}{u_2} \right)^{2-3n_2} \left(\frac{a_2 d}{v_2} \right)^{n_2} \left(\frac{d}{x} \right)^{1-n_2} \frac{\Delta p_{2,a}}{p_2}$$

$$= -\frac{2\gamma_2}{1-n_2} \left[\frac{FL_2 (u_s/a_2)^{1-2n_2}}{1 + \frac{(u_s/a_2)}{M_2}} \right]^{n_2} \left[1 + \frac{\xi_c}{x} C - \gamma_{32} \frac{1-n_2}{1-n_3} \frac{L_{32} D}{a_{32}} \left(\frac{M_2 \right)^{1+3(n_2-n_3)} \left(1 + \frac{u_s}{M_2} \right)^{1+n_2-n_3}}{\left(\frac{a_2}{u_s} \right)^{n_3-n_2} (1+M_3+a_{43})} \frac{v_3^{n_3}}{v_2^{n_2}} x^{n_2-n_3} \right] \times \left(1 - CE \frac{\Delta p_{2,c}}{\Delta p_{2,a}} \right)^{-1} \quad (\text{F6})$$

The corresponding change in shock Mach number can be found from equation (C5). Appropriate values for L and n are given in appendixes D and E.

If $n_2 = n_3$ and $CE \Delta p_{2,c} / \Delta p_{2,a}$ is assumed not to vary with x , then equation (F6) indicates that $\Delta p_{2,c} / \Delta p_{2,a} = (\xi_c/x)^{1-n_2}$ and

$$CE \frac{\Delta p_{2,c}}{\Delta p_{2,a}} = CE \left(\frac{\xi_c}{x} \right)^{1-n_2} \quad (\text{F7})$$

Equation (F7) indicates $CE \Delta p_{2,c} / \Delta p_{2,a}$ to be independent of x and is therefore consistent with the original assumption to this effect. Substitution of equation (F7) into equation

It can be shown that $\Delta p_{3,a}^+ = 0$ in the present case. Moreover, $p_2 = p_3$. The expression for $\Delta p_{2,a}$ can then be expressed as

$$\frac{1}{F} \frac{a_2 d}{2\gamma_2} \frac{\Delta p_{2,a}}{p_2} = \left[\frac{1}{1+M_2} \int_{\xi_b}^x v_2 d\xi + \frac{C}{1-M_2} \int_{\xi_b}^{\xi_c} v_2 d\xi + \frac{\gamma_{32} D}{a_{32}(1+M_3)} \int_{\xi_a}^{\xi_b} v_3 d\xi \right] \times \left(1 - CE \frac{\Delta p_{2,c}}{\Delta p_{2,a}} \right)^{-1} \quad (5)$$

In appendixes D and E it is shown that for wholly laminar or wholly turbulent boundary layers

$$\left. \begin{aligned} v_2 &= -L_2 \left[\frac{u_2^2/u_s}{1-(u_2/u_s)} \right]^{1-n_2} \left(\frac{v_2}{u_s \tau - \xi} \right)^{n_2} \\ v_3 &= L_3 \left[\frac{u_3^2/a_4}{1+(u_3/a_4)} \right]^{1-n_3} \left(\frac{v_3}{a_4 \tau + \xi} \right)^{n_3} \end{aligned} \right\} \quad (\text{F5})$$

where L and n are independent of τ and ξ . The values of L and n depend on whether the boundary layer behind a given wave is laminar or turbulent. Substituting equations (F5) into equation (5) and using equations (B3) yield

(F6) gives accurate results even when $n_2 \neq n_3$, since the major contribution to $\Delta p_{2,a}$ comes from the first term on the right side of equation (F6). The term $CE \Delta p_{2,c} / \Delta p_{2,a}$ represents the contribution to $\Delta p_{2,a}$ of all the characteristic lines of figure 2 other than lines ab , bc , and bd , and is referred to as the contribution of the reflected wave at point c in figure 6. It can be seen from figure 6 that this term is small and can probably be neglected in most cases.

If it is necessary to consider the boundary layer behind the shock (or expansion) wave as partly laminar and partly turbulent, then equation (5) must be integrated accordingly.

APPENDIX G

IDEAL SHOCK-TUBE RELATIONS

Shock-tube relations, assuming ideal flow, are presented herein for convenience. The formulas were obtained from reference 1. The notation $p_{12} = p_1/p_2$, $a_{32} = a_3/a_2$, and so forth, is again used.

Define

$$\begin{aligned} \alpha &\equiv (\gamma+1)/(\gamma-1) \\ \beta &\equiv (\gamma-1)/2\gamma \end{aligned}$$

Then

$$p_{14} = \frac{1}{p_{21}} \left[1 - (p_{21}-1) \sqrt{\frac{\beta_4}{\alpha_1 p_{21} + 1} \frac{(c_v T)_1}{(c_v T)_4}} \right]^{1/\beta_4} \quad (\text{G1a})$$

$$p_{34} = (p_{14} p_{21})^{1/\gamma_4} \quad (\text{G1b})$$

$$p_{21} = \frac{1 + \alpha_1 p_{21}}{\alpha_1 + p_{21}} \quad (\text{G1c})$$

$$T_{34} = a_{34}^2 = (p_{14} p_{21})^{2\beta_4} \quad (\text{G1d})$$

$$T_{21} = a_{21}^2 = \left[\frac{p_{21}(\alpha_1 + p_{21})}{1 + \alpha_1 p_{21}} \right] \quad (\text{G1e})$$

$$\frac{u_2}{a_1} = \frac{p_{21}-1}{\gamma_1 [\beta_1(\alpha_1 p_{21} + 1)]^{1/2}} \quad (\text{G1f})$$

$$\frac{u_3}{a_4} = \frac{1}{\gamma_4 \beta_4} \left[1 - (p_{14} p_{21})^{\beta_4} \right] \quad (\text{G1g})$$

$$\frac{u_s}{a_1} \equiv M_s = \left[\beta_1(1 + \alpha_1 p_{21}) \right]^{1/2} \quad (\text{G1h})$$

$$\frac{u_2}{a_2} \equiv M_2 = \frac{p_{21}-1}{\gamma_1 [\beta_1 p_{21}(\alpha_1 + p_{21})]^{1/2}} \quad (\text{G1i})$$

$$\frac{u_3}{a_3} \equiv M_3 = \frac{1}{\beta_4 \gamma_4} \left[(p_{14} p_{21})^{-\beta_4} - 1 \right] \quad (\text{G1j})$$

APPENDIX H

REYNOLDS NUMBERS AND TRANSITION

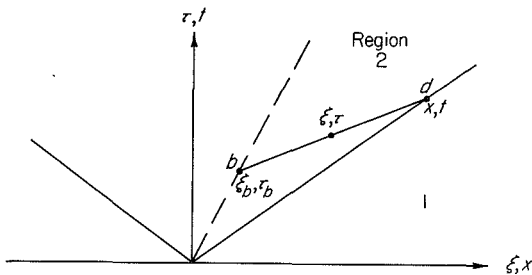
A Reynolds number characterizing the boundary-layer development in regions 2 and 3 of the shock tube is now developed.

$$\text{Region 2} \left(\frac{u_2}{u_s} \leq \frac{\xi}{u_s \tau} \leq 1 \right)$$

In the notation of reference 2, a Reynolds number characterizing the boundary layer behind a shock is defined therein as $Re = \frac{x}{\nu_w} \frac{(u_e - u_w)^2}{u_e}$. Using the transformations indicated by equations (D1) and arbitrarily basing ν on free-stream conditions, the Reynolds number for region 2 may be written as

$$Re_2 = \frac{u_2(u_s \tau - \xi)}{\nu_2} \frac{u_2/u_s}{(1 - u_2/u_s)} \quad (\text{H1})$$

where ξ, τ are the coordinates of a point in region 2 (following sketch).



Consider ξ, τ to be a point on the characteristic line through x, t (above sketch). The Reynolds number for points along this line, as a function of ξ , is (using eq. (B2))

$$Re_2 = \frac{u_2(x - \xi)}{\nu_2} \left(\frac{u_2/u_s}{1 - u_2/u_s} \right) \left(\frac{1 + M_2 - u_s/a_2}{1 + M_2} \right) \quad (\text{H2})$$

If the transition Reynolds number is known, equation (H2) can be used to determine the values of ξ at which transition occurs. The maximum Reynolds number in region 2 occurs at the contact surface ($\xi = \xi_b$) and equals

$$Re_{2,b} = \frac{a_1 x}{\nu_1} \left[\nu_{12} \left(\frac{u_2}{u_s} \right)^2 \left(1 + M_2 - \frac{u_s}{a_2} \right) M_s \right] \quad (\text{H3})$$

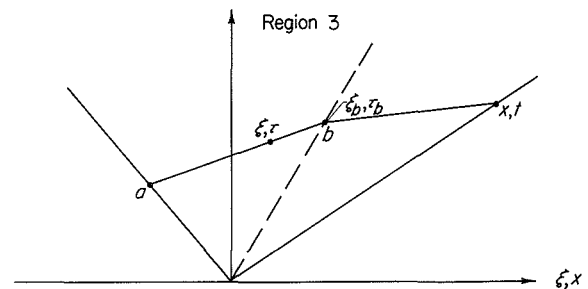
Equation (H3) can be used as a general index as to whether the boundary layer (along the characteristic line) is primarily laminar or primarily turbulent. A plot of $Re_{2,b}$ against M_s for air in region 1 (with $T_1 = 520^\circ \text{R}$) is given in figure 6.

The transition Reynolds number for the boundary layer behind a shock wave has not yet been established. In the absence of more accurate information, the transition Reynolds

number for incompressible flow over a semi-infinite flat plate [$Re = 0(0.5 \times 10^6)$] might be used to estimate the transition point behind a shock wave. That is, take $Re_2 = 0(0.5 \times 10^6)$ as a rough estimate for the transition Reynolds number. This is probably a conservative estimate for the strong-shock cases, since the large amount of heat transfer to the shock-tube walls may have a very stabilizing effect on the boundary layer.

$$\text{Region 3} \left(-1 \leq \frac{\xi}{a_4 \tau} \leq \frac{u_3}{a_4} \right)$$

For a point in region 3 (following sketch), the Reynolds



number as defined in reference 2 becomes (using eqs. (D2) and ν based on the free stream)

$$Re_3 = \frac{u_3(a_4 \tau + \xi)}{\nu_3} \frac{u_3/a_4}{1 + u_3/a_4} \quad (\text{H4})$$

For a point on the characteristic line influencing point x, t , the Reynolds number becomes

$$Re_3 = \frac{u_3 x}{\nu_3} \frac{u_3/a_4}{1 + u_3/a_4} \frac{1 + M_3 + a_{43}}{1 + M_3} \left[\frac{\xi}{x} + \left(\frac{1 + M_2 - u_s/a_2}{1 + M_3 + a_{43}} \right) \frac{a_4}{u_s} \right] \quad (\text{H5})$$

At the contact surface ($\xi = \xi_b$), equation (H5) has the value

$$Re_{3,b} = \frac{a_1 x}{\nu_1} \left[\nu_{13} \left(\frac{u_2}{u_s} \right)^2 \left(1 + M_2 - \frac{u_s}{a_2} \right) M_s \right] \quad (\text{H6})$$

The criterion $Re_3 = 0(0.5 \times 10^6)$ might be taken as a rough estimate for the transition Reynolds number behind the expansion wave.

The boundary-layer characteristics presented in appendixes D and E indicate a discontinuity in the boundary-layer profile across the contact surface. (Note that $Re_{2,b}/Re_{3,b} = \nu_3/\nu_2$.) This discontinuity does not actually occur, and the theoretical discontinuity thus represents a deficiency of the present method.

APPENDIX I

GENERATION OF PRESSURE WAVES BY WALL SHEAR AND HEAT ADDITION

The generation of pressure waves by body forces and by heat sources in one-dimensional flow is investigated, and the results are used to compare the method of the present report with that of reference 6.

WAVE GENERATION BY BODY FORCES AND HEAT SOURCES

Assume a uniform flow of pressure p , velocity u , and so forth, in a tube of constant cross section. This uniform flow is assumed to be slightly perturbed by weak body forces and heat sources. The equations of motion are (neglecting the possibility of mass sources, since this case is treated in eq. (1))

$$\left. \begin{aligned} \rho \left(\frac{\partial \Delta u}{\partial t} + u \frac{\partial \Delta u}{\partial x} \right) &= f - \frac{\partial \Delta p}{\partial x} \\ \frac{\partial \Delta \rho}{\partial t} + \rho \frac{\partial \Delta u}{\partial x} + u \frac{\partial \Delta \rho}{\partial x} &= 0 \\ \frac{\partial \Delta s}{\partial t} + u \frac{\partial \Delta s}{\partial x} &= \frac{q}{\rho T} \end{aligned} \right\} \quad (\text{I1})$$

where $f(x,t)$ is the body force per unit volume acting in the $+x$ -direction and $q(x,t)$ is the heat addition per unit volume per unit time. The symbol Δs represents the entropy perturbation of a particle and is related to the pressure and density perturbations by

$$\frac{\Delta s}{c_v} = \frac{\Delta p}{p} - \gamma \frac{\Delta \rho}{\rho} \quad (\text{I2})$$

The perturbation at any point x,t can be shown to equal

$$\left. \begin{aligned} \frac{\Delta p}{p} &= \frac{\Delta p^+}{p} + \frac{\Delta p^-}{p} \\ \frac{\Delta u}{a} &= \frac{1}{\gamma} \left(\frac{\Delta p^+}{p} - \frac{\Delta p^-}{p} \right) \\ \frac{\Delta s}{c_v} &= \frac{\gamma}{\rho u} \int_{-\infty}^x \frac{q \left(\xi, t - \frac{x-\xi}{u} \right)}{c_p T} d\xi \\ \frac{\Delta \rho}{\rho} &= \frac{1}{\gamma} \left(\frac{\Delta p}{p} - \frac{\Delta s}{c_v} \right) \end{aligned} \right\} \quad (\text{I3})$$

where

$$\frac{\Delta p^+}{p} = \frac{\gamma}{2\rho a(1+M)} \int_{-\infty}^x \left[\frac{q \left(\xi, t - \frac{x-\xi}{a+u} \right)}{c_p T} + \frac{f \left(\xi, t - \frac{x-\xi}{a+u} \right)}{a} \right] d\xi$$

$$\frac{\Delta p^-}{p} = \frac{\gamma}{2\rho a(1-M)} \int_x^{\pm\infty} \left[\frac{q \left(\xi, t - \frac{\xi-x}{a-u} \right)}{c_p T} - \frac{f \left(\xi, t - \frac{\xi-x}{a-u} \right)}{a} \right] d\xi$$

The upper limit on the integral for Δp^- is $+\infty$ or $-\infty$ depending on whether $M < 1$ or $M > 1$. Since equations

(1) and (I1) are linear, the solution for the case where mass sources are also present can be obtained by adding equation (2) to equation (I3). Note that an elemental heat or mass source generates a symmetric pressure-wave pattern (positive pressure waves propagating in the downstream and upstream directions), while an elemental body force generates an antisymmetric pressure-wave pattern (positive pressure waves propagating in the downstream direction and negative pressure waves propagating in the upstream direction).

COMPARISON WITH REFERENCE 6

In effect, reference 6 uses equations (I3) to find the shock attenuation in a shock tube. The value of q is obtained by averaging, across the tube cross section, the heat transfer at the wall and the viscous dissipation in the boundary layer. The value of f is found by averaging the wall shear across the tube cross section. Thus, if \bar{q}_w is the heat transferred into the boundary layer per unit wall area, H_w is the net dissipation in the boundary layer per unit wall area, and $\bar{\tau}_w$ is the shear per unit area exerted by the wall on the fluid (taken to be positive in the $+x$ -direction), then

$$\left. \begin{aligned} q &= \frac{l}{A} (\bar{q}_w + H_w) = \frac{4}{d} (\bar{q}_w + H_w) \\ f &= \frac{l}{A} \bar{\tau}_w = \frac{4}{d} \bar{\tau}_w \end{aligned} \right\} \quad (\text{I4})$$

Substituting equation (I4) into equation (I3) and integrating along appropriate characteristic lines should yield the same results for shock attenuation as those which were obtained in reference 6 from a somewhat different viewpoint. However, these results are not in agreement with the results obtained from equation (4) (the latter being the basis of the present report).

Equation (4) is based on v while equation (I4) contains terms relating to the heat transfer at the wall, viscous dissipation, and wall shear. But, from boundary-layer theory, it can be shown that v is dependent on terms related to the heat transfer at the wall, viscous dissipation, and the velocity profile (see, e. g., eqs. (D3a) and (D3c)). The heat-transfer and dissipation terms in equations (I4) and (4) play the same qualitative roles and, therefore, are not discussed further. However, the wall-shear term in equation (I4) in some cases has a sign opposite to that of the velocity-profile term in equation (4). Thus, these terms are not always in qualitative agreement, and this leads to discrepancies between the results obtained from equations (I4) and (4).

Consider, for example, the boundary layer in a shock tube for the case of negligible heat transfer and dissipation. For this case, v depends only on the velocity-profile term. Similarly, only the $\bar{\tau}_w$ term is retained in equation (4). The signs of v and $\bar{\tau}_w$ and of the resulting pressure perturbations in regions 2 and 3 of the shock tube are summarized in the following table:

Region	Sign					
	Perturbations based on v (eq (4))			Perturbations based on $\bar{\tau}_w$ (eq (I4))		
	v	Δp^+	Δp^-	$\bar{\tau}_w$	Δp^+	Δp^-
2	-	-	-	-	-	+
3	+	+	+	-	-	+

Thus, when heat transfer and dissipation are neglected, a perturbation solution based on v differs from a perturbation solution based on $\bar{\tau}_w$ in regard to the sign of the Δp^- waves in region 2 and the Δp^+ waves in region 3.

It may be concluded that attenuation solutions based on equation (I4) differ from those based on equation (4) in the

following respects: (1) The integration of equation (I4) along characteristic line ab tends to overestimate its contribution to shock attenuation, and (2) the integration of equations (I4) along characteristic line bc tends to underestimate its contribution to shock attenuation. For the limiting case $M_s \rightarrow 1$, the integrations along ab and bc are negligible, and equations (4) and (I4) give the same results for shock attenuation.

When the boundary layer is thin, it is obvious that the attenuation calculation should be based on equation (4). If the viscous shear affects the entire cross section (as for a long shock tube), there is no longer a core of potential flow and the solution should probably be based on equations (I4) (or on the characteristics method of ref. 6 when nonlinearities become important). The quantities $\bar{\tau}_w$, \bar{q}_w , and \bar{H}_w should then be based on unsteady pipe flow rather than on thin-boundary-layer theory. In practice, the boundary layer is generally sufficiently thin to permit the use of equation (4).

REFERENCES

1. Glass, I. I., and Patterson, G. N.: A Theoretical and Experimental Study of Shock-Tube Flows. *Jour. Aero. Sci.*, vol. 22, no. 2, Feb. 1955, pp. 73-100.
2. Mirels, Harold: Boundary Layer Behind Shock or Thin Expansion Wave Moving into Stationary Fluid. NACA TN 3712, 1956.
3. Mirels, Harold: Laminar Boundary Layer Behind Shock Advancing into Stationary Fluid. NACA TN 3401, 1955.
4. Donaldson, Coleman duP., and Sullivan, Roger D.: The Effect of Wall Friction on the Strength of Shock Waves in Tubes and Hydraulic Jumps in Channels. NACA TN 1942, 1949.
5. Hollyer, Robert N., Jr.: A Study of Attenuation in the Shock Tube. *Eng. Res. Inst., Univ. Michigan*, July 1, 1953. (U. S. Navy Dept., Office Naval Res. Contract No. N6-ONR-232-TO IV, Proj. M720-4.)
6. Trimpi, Robert L., and Cohen, Nathaniel B.: A Theory for Predicting the Flow of Real Gases in Shock Tubes with Experimental Verification. NACA TN 3375, 1955.
7. Van Dyke, Milton D.: Impulsive Motion of an Infinite Plate in a Viscous Compressible Fluid. *Jour. Appl. Math. Phys.*, vol. III, no. 5, 1952, pp. 343-353.
8. Maslen, Stephen H.: Second Approximation to Laminar Compressible Boundary Layer on Flat Plate in Slip Flow. NACA TN 2818, 1952.
9. Hartunian, Richard A.: Some Viscous Effects in Shock-Tube Flow. M. S. Thesis, Cornell Univ., June 1954.

TABLE I—EVALUATION OF $I_N = \int_0^1 \frac{z^N dz}{1+bz-cz^2}$

$\frac{c}{b+1}$	b																	
	-1.0	-0.8	-0.6	-0.4	-0.2	0	2	4	6	8	10	15	20	25	30	35	50	100
Reciprocal of I_7																		
0	0	2.1736	3.6804	5.1374	6.5741	8.0000	22.094	36.119	50.132	64.139	78.144	113.15	148.15	183.16	218.16	253.15	358.16	708.27
.1		2.0271	3.4086	4.7417	6.0549	7.3577	20.223	33.022	45.807	58.588	71.365	103.31	135.24	167.18	199.11	231.05	326.85	646.18
.2		1.8781	3.1333	4.3418	5.5311	6.7102	18.343	29.910	41.464	53.013	64.560	93.422	122.28	151.14	179.99	208.85	295.42	583.97
.3		1.7259	2.8537	3.9368	5.0014	6.0562	16.450	26.780	37.097	47.409	57.719	83.489	109.26	135.02	160.79	186.55	263.84	521.48
.4		1.5697	2.5688	3.5254	4.4643	5.3938	14.541	23.626	32.699	41.767	50.833	73.493	96.149	118.81	141.46	164.11	232.08	458.61
.5		1.4084	2.2770	3.1056	3.9175	4.7205	12.609	20.440	28.258	36.072	43.883	63.407	82.929	102.45	121.97	141.49	200.04	395.23
.6		1.2402	1.9756	2.6740	3.3570	4.0317	10.647	17.207	23.756	30.301	36.843	53.195	69.545	85.893	102.24	118.59	167.63	331.09
.7		1.0619	1.6602	2.2262	2.7763	3.3200	8.6368	13.904	19.160	24.412	29.663	42.785	55.905	69.023	82.142	95.260	134.61	265.78
.75		.96723	1.4947	1.9912	2.4748	2.9513	7.6046	12.211	16.807	21.400	25.991	37.465	48.937	60.408	71.878	83.347	117.76	232.45
.8		.86717	1.3217	1.7478	2.1621	2.5699	6.5450	10.477	14.400	18.319	22.237	32.028	41.817	51.605	61.393	71.180	100.54	198.41
.85		.75932	1.1377	1.4907	1.8331	2.1698	5.4447	8.6809	11.909	15.134	18.358	26.414	34.469	42.523	50.576	58.629	82.787	163.31
.9		.63882	.93571	1.2111	1.4775	1.7390	4.2764	6.7811	9.2791	11.775	14.269	20.502	26.733	32.964	39.195	45.425	64.115	126.41
.95		.49249	.69708	.88539	1.0669	1.2448	2.9656	4.6622	6.3539	8.0438	9.7328	13.953	18.173	22.392	26.610	30.829	43.484	85.666
.975		.39446	.54262	.67831	.80885	.93665	2.1715	3.3885	4.6019	5.8139	7.0253	10.052	13.079	16.105	19.130	22.156	31.233	61.487
1.0	↓	0	0	0	0	0	0	0	0	0	0	0	0	0	0	0	0	0
Reciprocal of $I_7 - I_8$																		
0	0	24.251	36.772	48.725	60.423	72.000	185.42	297.85	410.06	522.18	634.26	914.39	1194.4	1474.5	1754.5	2033.9	2874.6	5680.4
.1		23.108	34.705	45.758	56.577	67.262	171.91	275.59	379.07	482.45	585.80	844.09	1102.3	1360.5	1618.7	1876.9	2651.5	5233.2
.2		21.940	32.604	42.751	52.674	62.467	158.29	253.18	347.87	442.48	537.04	773.38	1009.7	1245.9	1482.2	1718.4	2427.1	4789.3
.3		20.743	30.459	39.691	48.705	57.604	144.54	230.57	316.41	402.17	487.89	702.12	916.30	1130.5	1344.6	1558.7	2201.1	4342.4
.4		19.509	28.262	36.563	44.662	52.648	130.60	207.70	284.61	361.44	438.24	630.17	822.04	1013.9	1205.7	1397.6	1973.1	3891.3
.5		18.229	25.997	33.350	40.518	47.581	116.43	184.48	252.35	320.14	387.90	557.28	726.58	895.87	1065.2	1234.4	1742.2	3434.8
.6		16.889	23.642	30.024	36.239	42.359	101.94	160.78	219.46	278.09	336.67	483.08	629.44	775.78	922.11	1068.4	1507.4	2970.5
.7		15.465	21.161	26.537	31.767	36.916	86.973	136.38	185.64	234.85	284.03	406.91	529.77	652.59	775.41	898.23	1266.7	2494.7
.75		14.710	19.853	24.707	29.429	34.075	79.231	123.79	168.21	212.58	256.92	367.73	478.50	589.25	700.00	810.74	1142.9	2250.3
.8		13.914	18.482	22.796	26.992	31.121	71.236	110.81	150.27	189.67	229.06	327.46	425.84	524.20	622.56	720.91	1015.9	1999.4
.85		13.062	17.025	20.771	24.418	28.006	62.879	97.285	131.58	165.84	200.08	285.63	371.15	456.65	542.16	627.65	884.13	1739.0
.9		12.127	15.434	18.572	21.630	24.643	53.951	82.880	111.72	140.53	169.32	241.26	313.18	385.09	456.99	528.89	744.57	1463.5
.95		11.043	13.600	16.050	18.447	20.813	43.926	66.777	89.568	112.34	135.09	191.95	248.80	305.64	362.47	419.31	589.79	1153.1
.975		10.384	12.488	14.525	16.529	18.512	37.979	57.267	76.514	95.744	114.97	163.00	211.03	259.05	307.06	355.08	499.12	972.39
1.00	↓	0	0	0	0	0	0	0	0	0	0	0	0	0	0	0	0	0